Correspondence to:

S. L. Jarugula,
sreelekha.jarugula@noaa.gov

Ocean Mixed Layer Response to Two Post-Monsoon Cyclones in the Bay of Bengal in 2018

Sree Lekha Jarugula[1] 🔿 and **Michael J. McPhaden[1]** 🔿

[1]NOAA Pacific Marine Environmental Laboratory, Seattle, WA, USA

Abstract The Bay of Bengal (BoB) is characterized by a shallow (∼10–20 m deep) fresh layer associated with 40–60 m deep warm near-surface layer during the post-monsoon season (October–November). We use hourly observations from a moored buoy at 15°N, 90°E along with satellite and ocean analysis data sets to understand the evolution of the near-surface layer during the passage of two category-3 cyclonic storms: Cyclone Titli (7–11 October 2018) and cyclone Gaja (10–15 November 2018). The mooring was ∼200 km away to the right of the two cyclone tracks. A 15 day (22 September–7 October) break in the Indian summer monsoon resulted in clear skies, calm winds, and sea surface temperature warming (SST) by 2.8°C before Titli. During Titli, near-surface thermal stratification restricted vertical mixing to 20 m depth and limited SST cooling at the mooring. During passage of cyclone Gaja, fresh Irrawaddy River water associated with a subsurface warm layer was advected to the mooring by mesoscale eddy flow. Cyclone winds could not break through the near-surface density stratification associated with this river water. Shear associated with near-inertial currents led to delayed mixed layer deepening after the cyclone's passage but there was no cold wake along the track of Gaja due to mixing of subsurface warm water to the surface. We illustrate the relevant processes at work for the two cyclones based on mixed layer salt and heat balance at 15°N, 90°E. This study demonstrates the importance of ocean preconditioning and thermohaline stratification on SST evolution under the influence of post-monsoon cyclones in BoB.

Plain Language Summary The Bay of Bengal (BoB) is an active zone for genesis of tropical cyclones. During the post-monsoon season, the near-surface ocean in the Bay is stable due to presence of a thin, fresh layer of river water and the subsurface waters are generally warm. In this study, we use in-situ mooring, satellite, and ocean analysis data sets to understand how the preexisting temperature and the salinity structure of the ocean can influences the ocean's response to two severe tropical cyclones, Titli and Gaja, that occurred in the Bay during October–November 2018. In the case of Titli, we observe that warming of the sea surface prior to arrival of cyclone resulted in strong thermal stratification, which restricted vertical mixing to a depth of 20 m under strong cyclone winds. During the passage of Gaja, river water with a subsurface warm layer advected to the mooring location resulted in stable stratification, which did not allow cyclone-induced mixing. We observe a delayed deepening of the mixed layer to 40 m depth due to shear induced by inertial currents and near-surface warming after the passage of cyclone Gaja. This study demonstrates the importance of preexisting upper ocean temperature and salinity stratification for mixed layer evolution under post-monsoon tropical cyclones in the BoB.

1. Introduction

The Bay of Bengal (BoB) is an active zone for cyclogenesis with an average of three to four tropical cyclones developing in the region every year (Alam et al., 2003; Balaguru et al., 2014; Chaudhuri et al., 2019). There are primarily two cyclone seasons: Pre-monsoon (April–June) and post-monsoon (October–December). The upper ocean structure and preconditioning processes in the Bay prior to cyclone passage can be very different in these two seasons. During the pre-monsoon season, the near-surface layer is subjected to the springtime warming and the upper ocean is stratified mainly by temperature and partly by salinity (Sengupta et al., 2008). During the post-monsoon season, nearly 50% of the entire northern BoB is covered by freshwater discharged into the Bay from monsoonal rain and major rivers like the Ganga-Brahmaputra-Meghna, Irrawaddy, Godavari, Krishna, and Mahanadi (Sengupta et al., 2006, 2016; Sree Lekha et al., 2018). The near-surface ocean in October–December is characterized by a shallow salinity-stratified mixed layer less than 10 m deep, which caps a barrier layer deeper than 50 m. Thermal inversions develop in the northern BoB during the post-monsoon and winter seasons as the sea surface temperature (SST) cools and the subsurface ocean is warmed by the shortwave flux penetrating through the shallow salinity-stratified mixed layer (Kurian & Vinayachandran, 2006; Thadathil et al., 2016).

The ocean response to pre-monsoon and post-monsoon cyclones and the subsequent evolution of SST therefore depends significantly on the preconditioning of the ocean. For example, Yu and McPhaden (2011) show that prior to the passage of cyclone Nargis in April 2008, downwelling Rossby waves led to horizontal convergence of surface freshwater, which further led to an increase in the buoyancy and enhanced the sea surface height anomaly (SSHA) associated with the Rossby waves. The thin fresh layer allowed trapping of heat that warmed SST, which coincided with the high SSHA. Deepening of the mixed layer under intense cyclone winds reduces SST by several degrees and results in the formation of cold wakes along the cyclone track, which prevent the cyclone from further intensification (D'Asaro, 2003; Emanuel, 1999; Lin et al., 2003; Pasquero et al., 2021; Price, 1981; Zedler et al., 2002). In a salinity-stratified ocean with a thick barrier layer like the Bay of Bengal, SST does not cool under tropical cyclones in the post-monsoon season, creating favorable conditions for further intensification of the cyclones (Balaguru et al., 2012; Girishkumar & Ravichandran, 2012; Neetu et al., 2012; Sengupta et al., 2008). Due to the presence of thick barrier layer and high moisture availability in the post-monsoon season, the enthalpy flux across the air-sea interface is high, which favors intensification of cyclones even though the available tropical cyclone heat potential (TCHP) is lower compared to the pre-monsoon season (Vissa et al., 2013). Apart from warm SST, other atmospheric parameters, such as relative humidity and relative vorticity play a very important role in tropical cyclone intensification (Girishkumar et al., 2015; Li et al., 2013).

Several studies indicate an increase in frequency and intensity of the post-monsoon cyclones in the past decade (Balaguru et al., 2014; Jyoteeshkumar Reddy et al., 2021; Mohanty et al., 2012; Singh et al., 2000; Tiwari et al., 2022). Balaguru et al. (2014) attribute this increase to a rise in SST, ocean heat content, and moist static energy in the eastern Bay. There have been a few observational studies reporting the ocean response to tropical cyclones in the Bay of Bengal based on Argo data (Lin et al., 2009; Maneesha et al., 2012, 2021; McPhaden, Foltz, et al., 2009), mooring observations (Chaudhuri et al., 2019; Navaneeth et al., 2019; Venkatesan et al., 2014), satellite chlorophyll data (Vijay Prakash et al., 2021), and Lagrangian float data (Kumar et al., 2019). In this study, we use a combination of hourly meteorological measurements, and surface and subsurface ocean variables measured at the 15°N, 90°E Research Moored Array for African-Asian-Australian Monsoon Analysis and Prediction (RAMA) mooring (McPhaden, Meyers, et al., 2009), along with the Soil Moisture Active Passive (SMAP) satellite sea surface salinity (SSS), satellite microwave optimally interpolated SST (OISST), Argo profile data, and three-dimensional ocean reanalysis data to study the upper ocean response and space-time evolution of the near-surface temperature and salinity during the passage of two very severe tropical cyclones, Titli and Gaja, in the Bay of Bengal during October–November 2018. Both Titli and Gaja were categorized as very severe cyclonic storms; they caused severe destruction, flooding, and claimed several lives in Orissa, Andhra Pradesh, and Tamil Nadu (IMD Report, 2018).

This study is unique in utilizing observational data from several platforms to investigate the contrasting differences between the two prominent cyclones in terms of ocean preconditioning and the interplay between the different upper ocean processes that lead to mixed layer deepening and SST evolution in response to strong cyclonic wind forcing. In Section 2, we discuss the data sets used in this study and methods used for analysis. Section 3 includes the main results where we discuss the surface heat and freshwater fluxes estimated at the mooring and the mixed layer temperature and salinity evolution during the passage of cyclones Titli and Gaja. Finally, the main findings of the study are summarized in Section 4.

2. Data and Methods

We use high-resolution hourly observations from the 15°N, 90°E RAMA mooring during the deployment period 7 June 2018–30 July 2019. The mooring was equipped with several sensors to measure the meteorological data and the radiation fluxes, Seabird SBE37 MicroCAT Conductivity Temperature (CT) sensors at selected depths in the upper 500 m to measure the temperature, salinity. The CT sensor measures temperature and salinity with an accuracy of ± 0.002°C and ± 0.02 practical salinity scale (pss), respectively (Freitag et al., 2001, 2016). Temperature measurements are available at 1, 10, 16, 20, 40, 50, 60, 80, 100, 120, 140, 180, 300, and 500 m depths, while the salinity data are available at 10, 16, 20, 40, 50, 60, 100, and 140 m depths (the 1 m salinity sensor unfortunately failed in July 2018). The mooring has a downward-looking Teledyne RDI 300 kHz Acoustic Doppler Current Profiler (ADCP) mounted on the surface buoy at 2 m depth to measure the ocean current velocity in the 6–70 m depth range with a 2 m vertical resolution. The ocean current profiles and directions are measured with an accuracy of ± 5 cm s^{-1} and ± 2.5°, respectively. Apart from the regular processing and data quality

checks done by the Global Tropical Moored Buoy Array (GTMBA) group at the Pacific Marine Environmental Laboratory (PMEL), the ADCP data are also corrected for errors resulting from backscattering of the signal due to several other sensors mounted below the ADCP on the mooring line. This correction is made by removing the data at depths where the error velocity is high and the zonal, meridional velocity profiles are biased toward zero velocity. All data shallower than 16 m were flagged, and after editing out data contaminated by backscatter at deeper depths, we linear interpolated to fill gaps in the current profile (Plimpton et al., 1997, 2004). Using this method, we find that about 25% of the data were contaminated due to backscattering at depths below 16 m, so we eliminated those data points.

The rain sensor on the mooring stopped working during the deployment, so we use the daily 0.25° gridded rainfall from the multi-satellite Tropical Rainfall Measuring Mission (TRMM) 3B42v7 data set (Huffman et al., 2007, 1998–present). In addition to these data sets, we also use daily 8-day running mean Level 3 version 4 SSS from the SMAP satellite available from May 2015 to present. SMAP SSS data with an original 70 km spatial resolution are resampled onto a 0.25° Earth grid using a Backus-Gilbert type optimum interpolation (Fore et al., 2016). We also use the daily 0.25° satellite microwave Optimum-Interpolation Sea Surface Temperature (OISST) product from the Remote Sensing Systems (Udaya Bhaskar et al., 2013), a merged satellite data set that includes SST measured from the Tropical Rainfall Measuring Mission Microwave Imager (TRMM-TMI) and the Advanced Microwave Scanning Radiometer–Earth Observing System (AMSR-E) satellite radiometers. Likewise, we use daily 0.25° surface Archiving, Validation and Interpretation of Satellite Oceanographic (AVISO) geostrophic currents (Saraceno et al., 2008). Apart from the mooring and satellite observations, we use about 55 temperature and salinity profiles from Argo floats within 1° × 1° box centered around the 15°N 90°E taken from the Global Argo Data Repository to validate the mixed layer depth and isothermal layer depth calculation at the mooring location.

We also use salinity, temperature, and velocity data from a 3D global ocean physics analysis and forecast product (Global_Analysis_Forecast_PHY_001_030) generated from the Nucleus for European Modeling of the Ocean (NEMO) model v3.1 with a 1/12° horizontal resolution and 50 vertical levels and atmospheric forcing from the European Center for Medium-Range Weather Forecasts (ECMWF) Integrated Forecast System (IFS); the temporal coverage is 1993–present (Chassignet et al., 2018). The model assimilates the satellite altimeter data, in situ temperature and salinity profiles from Argo, Operational Sea Surface Temperature and Ice Analysis (OSTIA) SST, which comprises of in situ observations and satellite data provided by the Group for High Resolution Sea Surface Temperature (GHRSST). The model does not assimilate satellite SSS. The ocean analysis data set has a good representation of the mesoscale circulation in the Bay of Bengal and the large-scale lateral gradients in temperature and salinity. However, at 15°N, 90°E, the ocean analysis fails to accurately represent the mixed layer evolution under the tropical storms and has significant biases in temperature and salinity as compared to the mooring measurements. In this study, we therefore use the ocean analysis only for the purposes of providing qualitative field views of temperature and salinity, checked against satellite observations where appropriate, to help us assess features such as salinity advection by mesoscale flow.

In Section 3, we estimate the terms in the mixed layer heat and salt balance to understand the processes contributing to the evolution of mixed layer temperature and salinity in response to the surface forcing during the passage of cyclones. Mixed layer depth (MLD) definition is based on either a net change in a physical property like temperature, salinity, or potential density at a depth relative to the surface or by a critical value of the gradient in a physical property at depth (Rao & Sivakumar, 2003). Past studies have used various definitions of MLD based on density criteria in the BoB. Shroyer et al. (2020) define mixed layer depth as the depth at which potential density exceeds the surface value by 0.03 kg m^{-3} for analysis of ship-based measurements to study the upper thermohaline structure in the BoB. Chaudhuri et al. (2019) use the MLD density criterion as 0.05 kg m^{-3} to study ocean response to tropical cyclone Phailin using moored observations from the northern Bay of Bengal. Other studies used MLD criteria as 0.125 and 0.15 kg m^{-3} (Girishkumar et al., 2017; Sree Lekha et al., 2020).

Following Scannell and McPhaden (2018), we validate the different potential density criteria for MLD definition at 15°N RAMA mooring by using 55 Argo profiles available in a 1° × 1° box centered around the mooring location during the deployment period. The Argo profiles with a vertical sampling resolution in the range 0.7–2 m have been regridded to a uniform 1 m vertical resolution. The scatterplots in Figure 1 show MLD calculated from the Argo data at a 1 m vertical resolution versus MLD from Argo data subsampled at mooring measurement depths (10, 16, 20, 40, 50, 60, and 100 m) using 0.03, 0.05, and 0.125 kg m^{-3} potential density criteria.
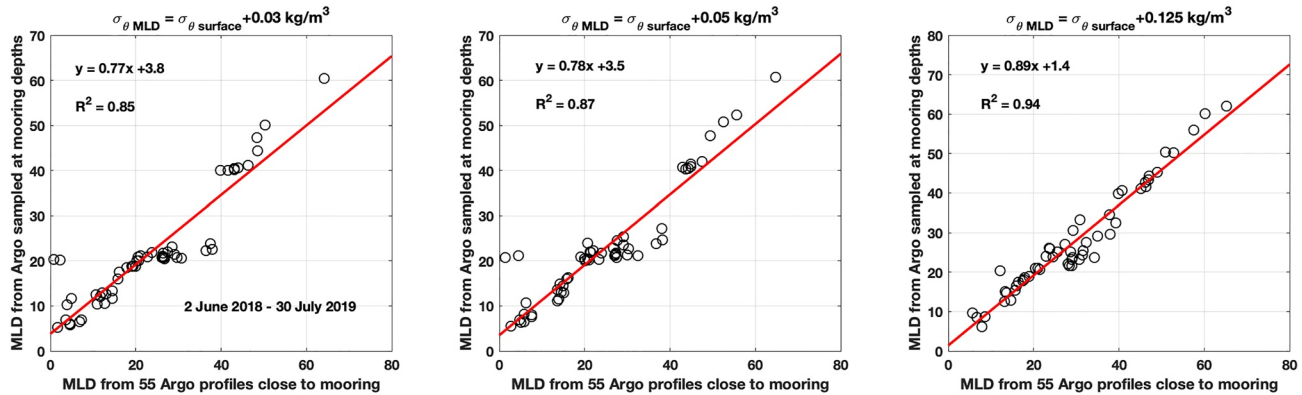
Figure 1. Scatterplot between mixed layer depth (MLD; m) calculated from 55 Argo profiles within $1° \times 1°$ box centered around 15°N, 90°E at an original depth resolution (x axis) and from Argo profile data sampled at mooring measurement depths (y axis) during the mooring deployment period June 2018 to July 2019 using the criteria when the potential density (σ_θ; kg m^{-3}) exceeds σ_θ at the surface by (a) 0.03 kg m^{-3}, (b) 0.05 kg m^{-3}, and (c) 0.125 kg m^{-3}. The linear regression line (red), equation, and correlation coefficient (R^2) are shown.

Linear regression analysis indicates a correlation of 0.94 between the two MLDs for the 0.125 kg m^{-3} density criterion (Figure 1c) as compared to 0.85 and 0.87 for the 0.03 and 0.05 kg m^{-3} criteria (Figures 1a and 1b). Root Mean-Squared Error (RMSE) is 1.5 m within depth range of 1–20 m, 5 m in the 20–40 m range, and 3 m in 40–70 m range for the 0.125 kg m^{-3} density criterion. Hence, we calculate MLD from the 15°N mooring observations based on 0.125 kg m^{-3} density criterion and adjust MLDs obtained from the mooring data using the regression equation obtained from the Argo data analysis to adjust for a coarse vertical sampling resolution in the mooring data. The isothermal layer depth (ILD) is defined as the depth where the temperature is cooler than the surface temperature by 0.4°C; it is estimated using the temperature criterion: $T_{ILD} = T_{surface} - 0.4°C$. The ILD criterion is chosen such that it matches the mixed layer depth in the absence of vertical salinity gradient. We use T/S measurements from 10 m depth onward to compute both MLD and ILD. We have validated the ILD with near-by Argo profile data similar to the validation of MLD and find a correlation of 0.82 between the two ILDs using the above-mentioned temperature criterion.

We define the vertical density ratio $R = \frac{\alpha \Delta T}{\beta \Delta S}$, where α, β are coefficients of thermal expansion and haline contraction, respectively; ΔT and ΔS are the changes in temperature and salinity in depth, respectively (Cole et al., 2010; Figueroa, 1996; Rudnick & Ferrari, 1999). Values of $R = 1$ suggest equal density compensation by the salinity and temperature gradients, $R > 1$ implies temperature dominance, and $R < 1$ implies salinity dominance. The square of velocity shear is defined as $S^2 = \left(\frac{dU}{dz}\right)^2 + \left(\frac{dV}{dz}\right)^2$ where U and V are the zonal and meridional velocities and z is the depth. The stability of near-surface layer is measured by the square of Brunt Vaisala frequency $N^2 = -\frac{g}{\rho}\frac{d\rho}{dz}$ where g is acceleration due to gravity and ρ is density of seawater as a function of depth z. A Richardson number (Ri = N^2/S^2) is used to determine the stability of the water column. Linear theory suggests that the water column is subject to instabilities and turbulence mixing occurs when Ri < 0.25.

3. Results and Discussion

Tropical cyclone Titli traversed the Bay of Bengal during 7–11 October 2018 (Figures 2a and 2b). The Indian Meteorological Department categorized Titli as a very severe cyclonic storm (VSCS), which originated from a low-pressure system over the southeastern BoB on 7 October 2018, then intensified into VSCS in the north central Bay on 10 October 2018 as it moved northwestward and made landfall on the southern coast of Odisha near Palasa (18.8°N, 84.5°E) on 11 October 2018. The maximum sustained wind speed associated with cyclone Titli was 140–150 km hr^{-1} with gusts at 165 km hr^{-1}. Figures 2a and 2b shows the basin-scale SSS and SST response to cyclone Titli. SMAP satellite data show a maximum of 2.5 pss rise in SSS off the coast of Orissa as Titli strengthened into a severe cyclonic storm. We also observe a cold wake along the track of cyclone Titli, which shows a maximum surface cooling of about 3.5–4°C closer to Orissa coast. Titli traversed 200 km left of the 15°N, 90°E RAMA mooring on 9 October 2018 when the cyclone transformed from a deep depression into a cyclonic storm with a translational speed of about 10 km hr^{-1}. The impact of surface forcing associated with cyclone Titli lasted at the mooring location for about 5 days.
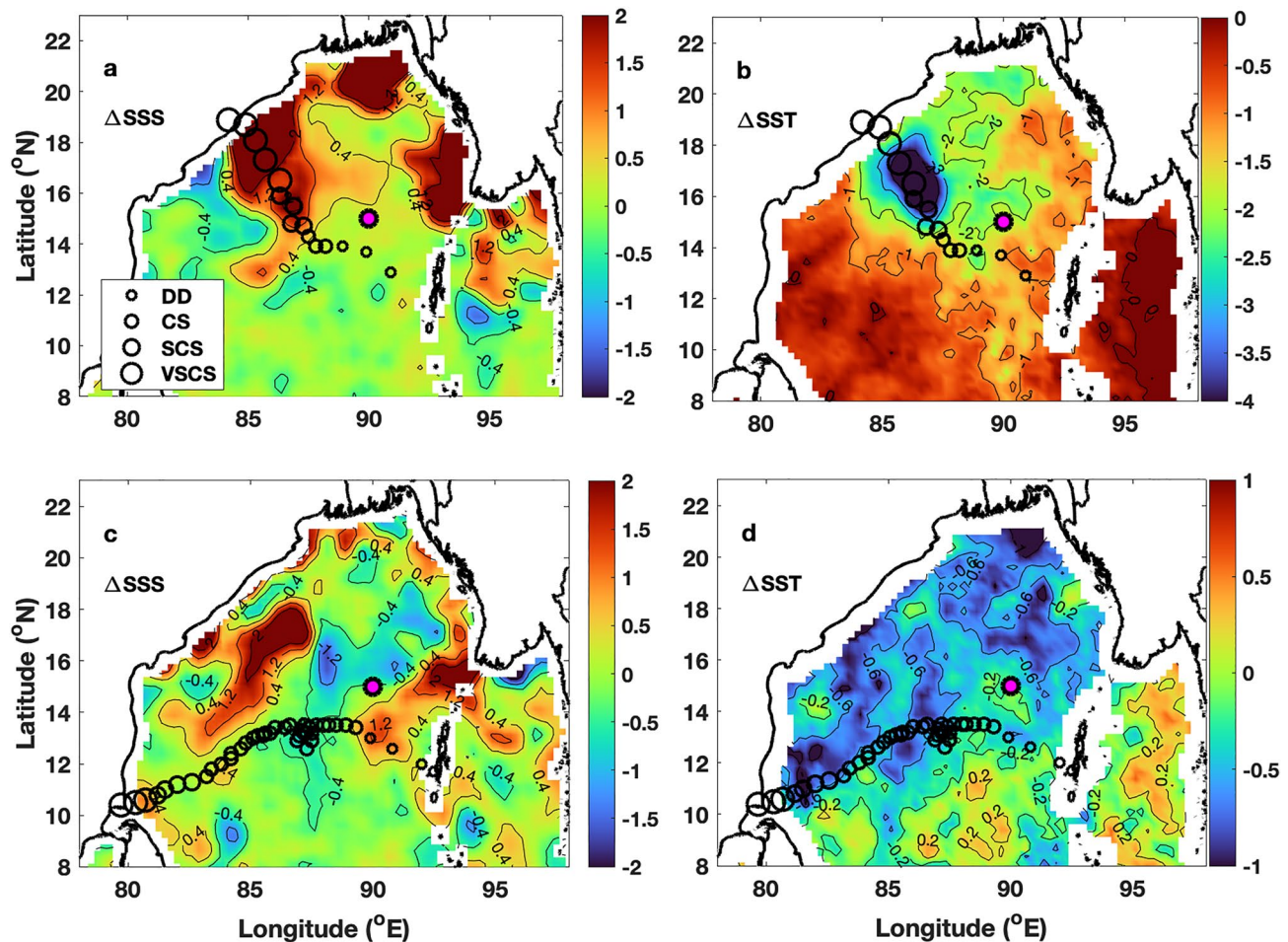
Figure 2. Spatial maps of difference in (a) daily 8 day running mean Soil Moisture Active Passive (SMAP) satellite sea surface salinity (pss; color and contours) and (b) daily satellite microwave optimally interpolated sea surface temperature (OISST, °C; color and contours) between 11 October and 7 October 2018. Panels (c and d) are same as (a and b) but the difference is between 15 November and 8 November 2018. The three-hourly Indian Meteorological Department track (data black circles) of cyclone Titli and cyclone Gaja are shown in panels (a and b) and (c and d), respectively. The size of circles along cyclone tracks represents the intensity of the cyclone ranging from deep depression (DD), which are the smallest circles to Very Severe Cyclonic Storm (VSCS), which are the largest. The 15°N, 90°E Research Moored Array for African-Asian-Australian Monsoon Analysis and Prediction mooring (pink dot) shown in all panels.

Cyclone Gaja, on the other hand, originated from a low-pressure system formed in the Gulf of Thailand on 8 November 2018, about a month later than cyclone Titli. As the system moved northwestward, it intensified into a cyclonic storm on 11 November in the central Bay of Bengal. On 12–13 November, the cyclone track curved into an anticyclonic loop and then the cyclone moved southwestward further intensifying into a VSCS before making landfall at Nagapattinam (10.45°N, 79.8°E) on the coast of Tamil Nadu on 15 November 2018 (Figures 2b and 2d). The cyclone continued to move westward over the land, weakened into a depression over central Kerala but again intensified into a deep depression over the southeast Arabian Sea and the Lakshadweep islands (IMD Report, 2018). The post-storm minus pre-storm satellite maps do not show any significant change in surface salinity and temperature along the track of cyclone Gaja. We observe freshening around the 15°N RAMA mooring and cooling over the entire northern and western BoB by about 0.6°C, which is part of the boreal winter-time seasonal cooling (Thadathil et al., 2002, Figures 2c and 2d). We discuss the reason for absence of distinct cold wake in case of cyclone Gaja in Section 3.2. Gaja's closest approach to the 15°N RAMA mooring—193 km to the south (left) was on 11 November 2018 where it intensified into a cyclonic storm with a maximum sustained surface wind speed of 74 km hr^{-1} and a translational speed of 10 km hr^{-1}. The strong winds associated with cyclone Gaja persist at the mooring location for 3 days, slightly shorter as compared to cyclone Titli.

During the time the mooring was deployed (June 2018–July 2019), five severe cyclonic storms traversed the BoB, and a sharp episodic increase in the hourly wind stress magnitude at the 15°N mooring was observed in
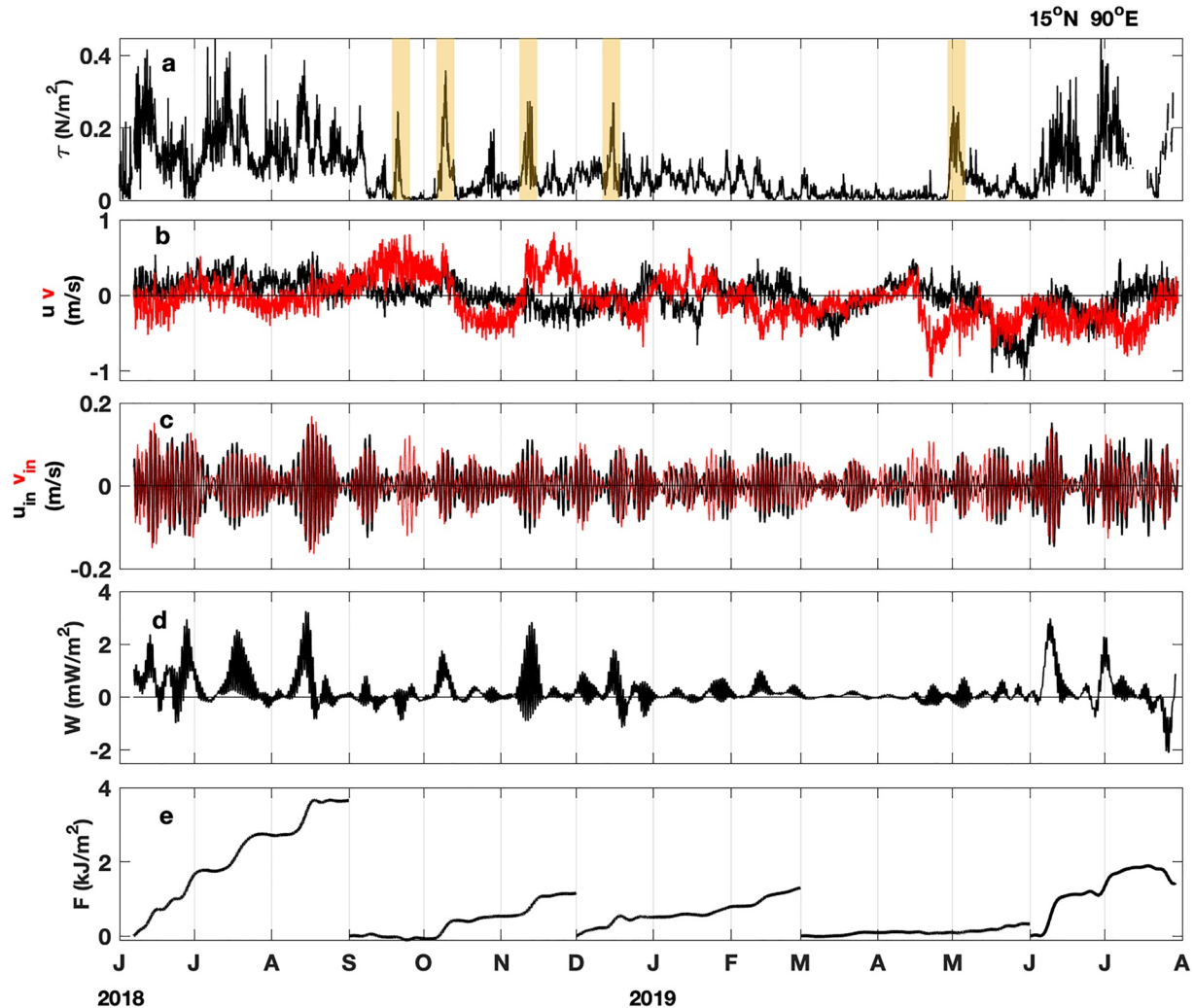
Figure 3. (a) Moored hourly wind stress magnitude (τ; N m^{-2}), (b) moored hourly ADCP zonal velocity U (m s^{-1}; black) and meridional velocity V (m s^{-1}; red) measured at 16 m depth, (c) 38–54 hr band-passed hourly zonal velocity u_{in} (m s^{-1}; black) and meridional velocity v_{in} (m s^{-1}; red) (d) Flux of near-inertial energy W (units: mW m^{-2}) = $\tau_{IN} \cdot U_{IN}$ where τ_{IN} is inertial wind stress and U_{IN} is the inertial 16 m depth velocity and (e) Integrated energy flux F (kJ m^{-2}) = $\int$W dt. Yellow shading in panel (a) marks the passage of tropical cyclones Daye (18–20 September 2018), Titli (7–11 October 2018), Gaja (10–15 November 2018), Pethai (13–17 December 2018), and Fani (28 April–3 May 2019).

response to these five storms (Figure 3a). Apart from the cyclonic disturbances, strong winds were observed during the southwest monsoon season (June–September) associated with monsoon lows and depressions moving over the BoB. The local inertial period at the mooring location is 46.2 hr. We band-pass the wind stress and ADCP velocity measured at the mooring using 38–54 hr Butterworth filter to obtain inertial wind stress and inertial currents (Figures 3b and 3c). Inertial currents are set up by the strong winds associated with monsoon depressions and cyclonic storms. We compute the total flux of the near-inertial energy input by the winds into the ocean near-surface layer using W = $\tau_{IN} \cdot U_{IN}$ where τ_{IN} is inertial wind stress and U_{IN} is the inertial velocity at 16 m depth (Figure 3d). The time integral of energy flux (F) shows increase in energy flux in several short-lived events associated with strong winds (Figure 3e). At the mooring location, we find that the total near-inertial energy input into the near-surface layer is about 8 kJ m^{-2} during this 1-year period. About 64% of the total energy input comes from the summer monsoon season. Tropical cyclones Titli and Gaja contribute to about 8% of the total near-inertial energy input. We do not always observe an increase in the near-inertial energy flux in response to strong winds as in the case of cyclone Fani during 28 April–3 May 2019 for instance. This could be a result of nonresonant response of the mixed layer to the cyclone winds. The flux of kinetic energy from winds to the mixed layer occurs when the rotating wind stress is in the same direction as the mixed layer inertial motions leading to
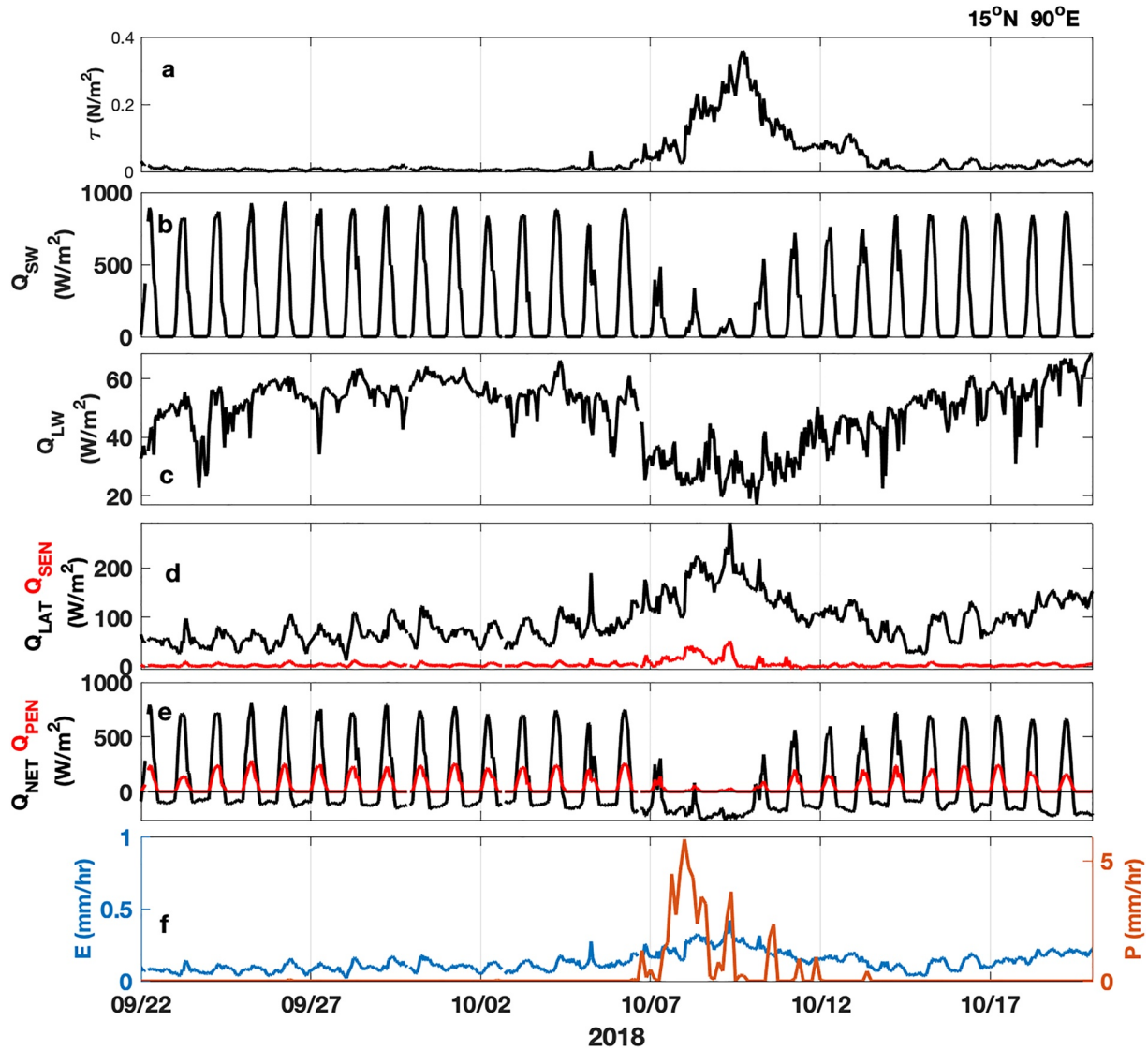
Figure 4. Moored observations of hourly (a) wind stress magnitude (τ; N m^{-2}) (b) net shortwave radiation flux (Q_{SW}; W m^{-2}), (c) net longwave radiation flux (Q_{LW}; W m^{-2}), (d) latent heat flux (Q_{LAT}; W m^{-2}; black), sensible heat flux (Q_{SENS}; W m^{-2}; red), (e) total net heat flux (Q_{NET}; W m^{-2}; black), penetrative shortwave flux below the MLD (Q_{PEN}; W m^{-2}; red), (f) evaporation rate (E; mm hr^{-1}; blue) and TRMM 3 hourly 3B42v7 precipitation rate (P; mm hr^{-1}; red) at 15°N 90°E during 22 September–20 October 2018. Please note that the y axis is different for P and E.

a resonant response (D'Asaro, 1985; Mickett et al., 2010; Pollard & Millard, 1970). In the following subsections, we focus on understanding the mixed layer response to cyclones Titli and Gaja primarily because: (a) both these cyclones occurred in the post-monsoon season (October–November) and belonged to the category of Very Severe Cyclonic Storms (VSCS) and (b) the tracks of these two cyclones were closest to the 15°N RAMA mooring as compared to other cyclones.

3.1. Ocean Response to Cyclone Titli

Figure 4 shows the heat and freshwater fluxes measured at the 15°N, 90°E RAMA mooring during the passage of cyclone Titli. The wind stress magnitude measured at the mooring increased from nearly zero to about 0.35 N m^{-2} and wind speed increased by 12 m s^{-1} in 4 days as the cyclone approached to within about 200 km to the left of the mooring location on 9 October 2018 (Figure 4a).

During 7–9 October, the net shortwave radiation flux was reduced by more than 500 W m^{-2} due to intense cloud cover. The penetrative shortwave radiation flux at depth z is estimated following Paulson and Simpson (1977)
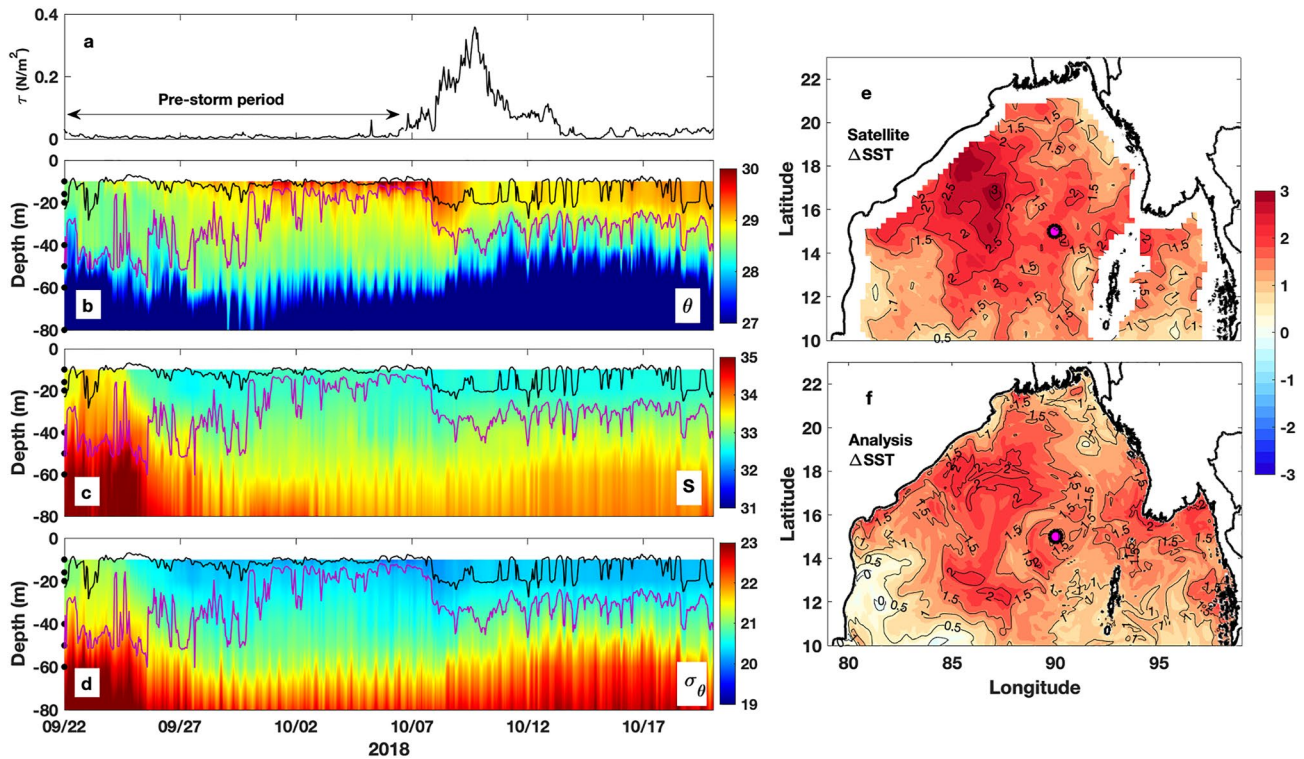
Figure 5. Moored observations of hourly (a) wind stress magnitude (τ; N m^{-2}), time-depth sections of (b) potential temperature (θ; ºC), (c) salinity (S; pss), and (d) potential density (σ_θ; kg m^{-3}) during 22 September–20 October 2018. The mixed layer depth (MLD; black) and isothermal layer depth (ILD; purple) and measurement depths (black dots) are shown in panels (b–d). Sea surface temperature warming (SST) difference (°C; color and contours) computed during the pre-storm period (5 October) minus the post-storm period (22 September); marked in panel (a)) using (e) the daily satellite microwave OISST and (f) daily global ocean analysis data. Location of 15°N, 90°E Research Moored Array for African-Asian-Australian Monsoon Analysis and Prediction mooring (pink dot) is shown. MLD is computed using the density criterion: $\sigma_{MLD} = \sigma_{surface} + 0.125$ kg m^{-3}. ILD is computed using the temperature criterion: $T_{ILD} = T_{surface} - 0.4$°C. The semidiurnal M2 tidal (12.5 hr) variability is prominent in temperature, salinity, and potential density at deeper depths below 40 m.

by using $Q_{PEN}(z) = Q_{SW} R e^{\frac{-z}{\zeta 1}} + Q_{SW}(1 - R) e^{\frac{-z}{\zeta 2}}$, where Q_{SW} is the net shortwave radiation flux (W m^{-2}), R is the albedo at ocean surface taken as 0.62, ζ_1 and ζ_2 are attenuation depths taken as 1.5 and 20 m, respectively (Parampil et al., 2016; Sree Lekha et al., 2020; Thangaprakash et al., 2016). The reduced net shortwave radiation and deepening of mixed layer to about 20 m depth (Figure 5a; discussed later in detail) during 7–9 October lead to reduction in the penetrative shortwave flux below the mixed layer (Figures 4b and 4e). The net heat flux that is defined as sum of net shortwave, net longwave, latent and sensible heat fluxes was about −250 W m^{-2} during the passage of the storm with a negative sign implying that the ocean is losing heat from the surface. The drop in latent heat flux by about −200 W m^{-2} is consistent with a slight increase in the rate of evaporation from the surface. The TRMM satellite rainfall data show the increased precipitation rate associated with cyclone Titli (Figure 4f). The last week of September and early October was a break period in the summer monsoon with calm wind conditions and clear skies. The wind stress magnitude during the pre-storm period (22 September–5 October 2018), prior to the arrival of cyclone Titli was nearly zero (Figure 5a) and the mean net heat flux during this period was about 126 W m^{-2}, which resulted in warming of SST by nearly 2.5°C (Figures 4e and 5b). The near-surface salinity during this period did not change significantly with SSS changes being less than 0.5 pss (Figure 5c). The potential density structure during this period closely resembled the structure of potential temperature suggesting a significant contribution of potential temperature to potential density as compared to that of salinity (Figures 5b and 5d).

The mean vertical density ratio during the pre-storm period in the upper 20 m depth was about 1.62 suggesting strong contribution of temperature to the near-surface density stratification. Spatial maps of SST observed from the microwave satellite and ocean analysis show warming of the entire BoB during the pre-storm period (Figures 5e and 5f). The maximum SST rise occurred to the northwest of the RAMA mooring, closer to the coast. The amplitude of SST warming is underestimated in certain locations by at least 0.5°C in the ocean analysis data
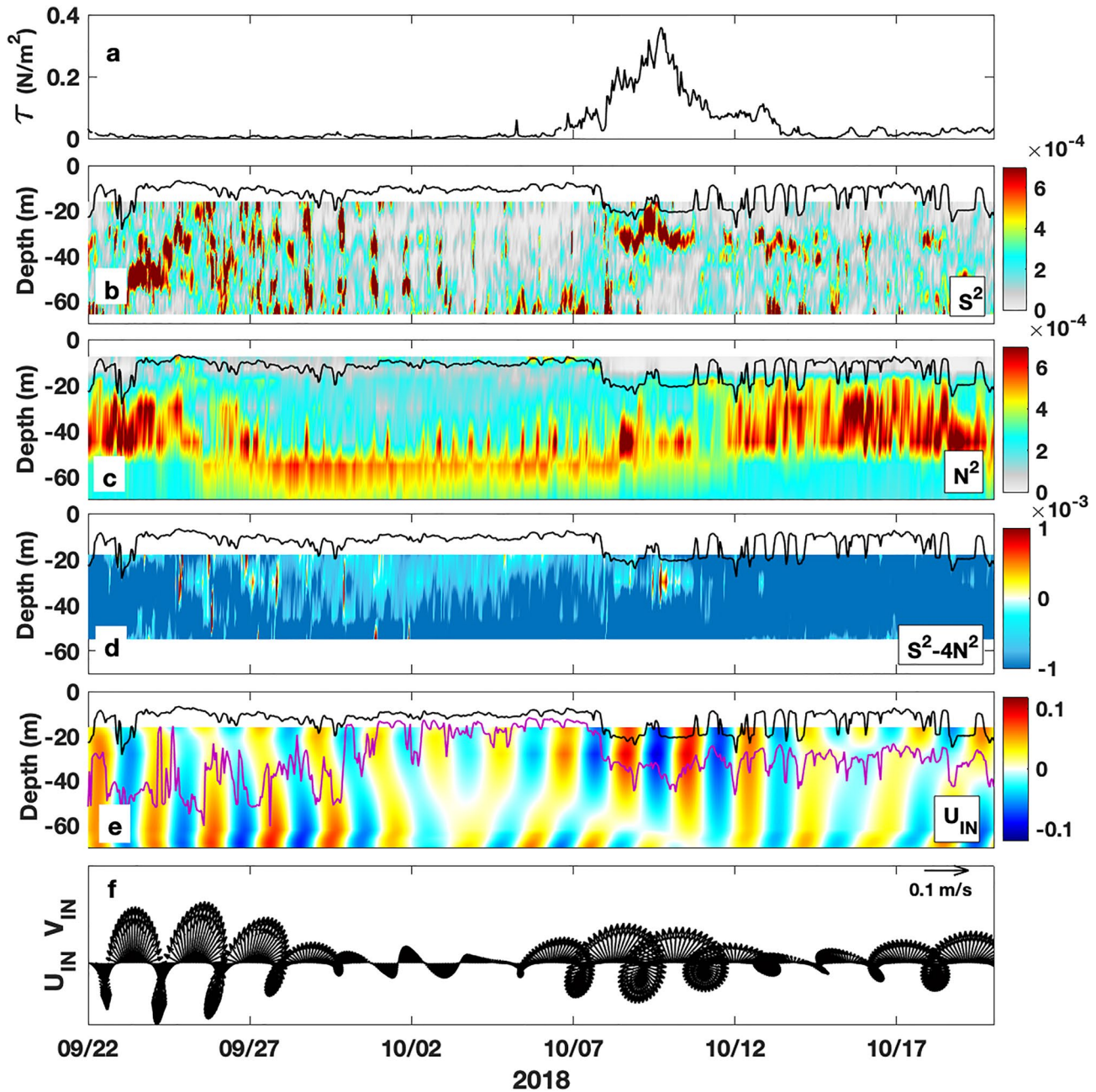
Figure 6. Moored observations of hourly (a) wind stress magnitude (τ; N m^{-2}), time-depth sections of (b) shear-squared (S^2; s^{-2}), (c) Brunt-vaisala frequency squared (N^2; s^{-2}), (d) reduced shear (S^2–4 N^2; s^{-2}), and (e) inertial zonal velocity (U$_{IN}$; m s^{-1}). MLD (m; black) and ILD (m; purple) are shown in panels (b–e). (f) Vector plot of zonal (U$_{IN}$; m/s) and meridional (V$_{IN}$; m s^{-1}) inertial currents during 22 September–20 October 2018 at 15°N, 90°E. A reference current vector of of 0.1 m/s is shown.

but the overall pattern of the SST warming agrees well with the satellite data. The mixed layer remained very shallow at 10 m during the pre-storm period but deepened to about 25 m depth as the winds strengthened in response to the cyclone. The barrier layer depth given by the difference between ILD and MLD was about 16 m during the passage of the cyclone.

We observe strong velocity shear at the base of mixed layer during the passage of cyclone (Figure 6b). The near-surface N^2 maximum during the pre-storm period is poorly represented in the data due to lack of high vertical resolution in the upper 20 m depth. The deeper N^2 maximum occurred between 40 and 60 m depth due to a sharp vertical gradient in temperature and density at the top of thermocline (Figure 6c). The mean bulk Ri at 18 m depth during the pre-storm period was about 1.91 and during the passage of storm (8–10 October) Ri

is 0.17. The reduced shear, defined as S^2–4 N^2, is greater than zero during the passage of storm (Figure 6d). However, it is important to note that these are bulk estimates and given the coarse resolution of the data in the upper 20 m, there is a high probability that we have underestimated the maximum values of N^2 and S^2. Nonetheless, this construct serves as a valuable index for the likelihood of shear induced mixing.

The strong cyclone winds generated strong near-inertial currents with an amplitude of about 8–9 cm s^{-1} during 8–11 October, which decayed in 2 days after the passage of cyclone (Figures 6e and 6f). Due to build-up of strong thermal stratification in the near-surface layer prior to the arrival of the storm, the mixed layer did not deepen beyond 25 m in spite of strong shear generated by the near-inertial currents (Figures 5 and 6). This shallow mixing resulted in SST cooling by about 2°C at the mooring. However, the maximum cooling (about 3.5°C) occurred along the track of Titli to the northwest of the mooring, probably because the cyclone rapidly intensified on 10 October while approaching the Orissa coast. Maneesha et al. (2021) show from Argo observations and a high-resolution NEMO model run that the cyclone-induced mixing in this region was restricted to the upper 50 m depth due to strong near-surface salinity stratification built up by the fresh water discharge from the Mahanadi River along the Orissa coast. Mohanty et al. (2021) use the Hurricane Weather Research and Forecasting (HWRF) model to understand the rapid intensification of cyclone Titli and they found that the sudden influx of moisture from lower tropospheric levels to mid-tropospheric levels led to an increase in humidity and further intensified the cyclone circulation. The near-inertial oscillations in the currents during the last week of September were not a local response to the wind forcing and are remnant features from the previous cyclone Daye (18–20 September 2018; Figure 6f). The track of cyclone Daye was to the right of the 15°N mooring and we did not observe significant near-inertial energy input by the local wind forcing associated with Daye (Figure 3e). Hence, the strong near-inertial currents observed in ADCP measurements at the mooring seem to be remotely forced.

3.1.1. Mixed Layer Heat and Salt Balance

To gain more understanding about the relevant processes at work responsible for the evolution of the mixed layer temperature and salinity, we construct the mixed layer salt and heat balance using the observations at 15°N RAMA mooring along with satellite data. The mixed layer salt balance is given by

$$\frac{\partial S}{\partial t} = (E - P)\frac{S}{h} - \left[u\frac{\partial S}{\partial x} + v\frac{\partial S}{\partial y}\right] + \epsilon$$

where $\frac{\partial S}{\partial t}$ is the local rate of change in mixed layer salinity (S); $(E - P)\frac{S}{h}$ is the freshwater forcing term where E and P are the rates of local evaporation and precipitation; $\left[u\frac{\partial S}{\partial x} + v\frac{\partial S}{\partial y}\right]$ is the horizontal advection term where u, v are the mixed layer average zonal and meridional velocity, $\frac{\partial S}{\partial x}$ and $\frac{\partial S}{\partial y}$ are the lateral gradients in salinity in zonal and meridional directions. The residual term ϵ is the difference between the tendency term and freshwater forcing and horizontal advection terms. It includes contributions from vertical advection, entrainment, and mixing processes, but also includes errors from all the explicitly estimated terms in the balance equation (Foltz & McPhaden, 2008). For computing the horizontal advection term, we used mixed layer average currents from the ADCP measurements at the mooring and lateral gradients in salinity from SMAP satellite SSS over 50 km spatial separation centered around 15°N, 90°E, that is, 25 km on either side of the mooring. The standard error is estimated based on the standard deviation of each term in the salt balance equation, which is computed using hourly moored observations of mixed layer average salinity, zonal and meridional velocity, rate of evaporation, TRMM hourly 3B42v7 rainfall rate, and the lateral gradients in salinity computed using the daily SMAP satellite data that are regridded to hourly values.

During the passage of cyclone Titli, the mixed layer salinity change was very small, less than 0.1 pss/day in magnitude (Figure 7a). The freshwater forcing term was negative during 7–11 October due to precipitation associated with cyclone Titli but we do not observe any significant drop in the mixed layer salinity during this period. This suggests that salty water was entrained into the mixed layer at times during Titli, but it appears to be an intermittent process and subject to uncertainty, given the smallness of the signal compared to Gaja (see below).

The corresponding mixed layer heat balance equation is given by

$$\frac{\partial T}{\partial t} = \frac{Q_{NET} - Q_{PEN}}{\rho C_p h} - \left[u\frac{\partial T}{\partial x} + v\frac{\partial T}{\partial y}\right] + \varepsilon$$
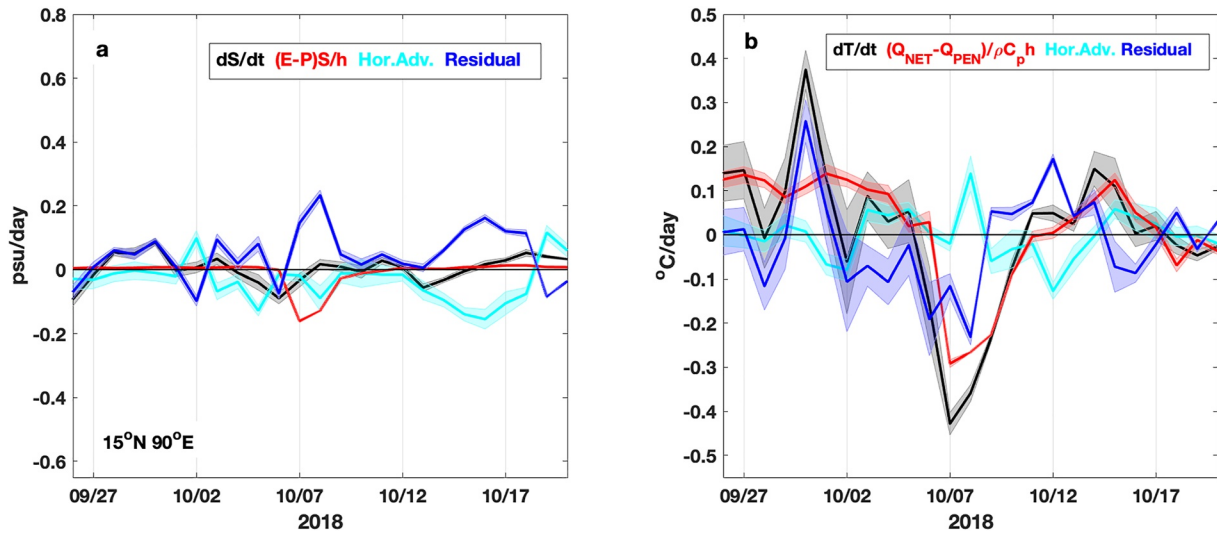
Figure 7. (a) Daily estimates of the rate of change in mixed layer salinity (dS/dt; black), freshwater forcing ($\frac{(E-P)S}{h}$; red), horizontal advection (cyan), and residual (blue) terms in the mixed layer salt balance equation during 26 September to 19 October 2018. Units in pss day^{-1}. (b) Daily estimates of rate of change in mixed layer temperature (dT/dt; black), surface heat forcing ($\frac{Q_{net}-Q_{pen}}{\rho C_p h}$; red), horizontal advection (cyan), and residual (blue) terms in the mixed layer heat balance equation. Units in °C day^{-1}. Shading in (a) and (b) represents one standard error in each term. The y axes in both panels are the same as in Figure 12. We estimate the standard error of each term in the balance equations on a single day conservatively as the standard deviation of the 24 hourly values for that particular day.

where $\frac{\partial T}{\partial t}$ is the temperature tendency term (°C day^{-1}); Q_{NET} is the net heat flux and Q_{PEN} is the net heat flux and penetrative shortwave radiation flux below the mixed layer (see Section 3.1) estimated using Paulson and Simpson (1977), ρ is density of seawater, C_P is the specific heat capacity, and h is the mixed layer depth. Horizontal advection is estimated using the mixed layer average ADCP currents u, v and lateral temperature gradients calculated from satellite microwave OISST at 50 km spatial separation centered around 15°N, 90°E. The residual term ε includes contributions from vertical advection, entrainment, and mixing processes, but also includes errors from all the explicitly estimated terms in the balance equation. The standard errors for each term are calculated in a similar manner as the errors in the salt balance equation.

During the preconditioning period (26 September–6 October 2018), warming of mixed layer was mainly due to the surface forcing as a result of clear skies and calm wind conditions associated with the monsoon break period (Figures 5 and 7b). During the passage of the cyclone, the mixed layer temperature dropped at the rate of 0.45°C day^{-1} as a result of heat loss from the surface and shear-induced mixing under strong cyclone winds, which deepened the mixed layer to a depth of about 25 m (Figure 7b).

3.2. Ocean Response to Cyclone Gaja

Cyclone Gaja traversed at a distance of about 193 km to the left of the 15°N RAMA mooring during 11–13 November 2018. The maximum hourly wind stress magnitude measured at the mooring was about 0.3 N m^{-2}. Due to looping of the cyclone track (Figures 1c and 1d), we observed rapid changes in the wind stress magnitude and direction during 10–13 November instead of a uniform gradual increase (Figure 8a). During the cyclone passage, the surface net heat flux was about −250 W m^{-2} due to a significant decrease in the shortwave radiation flux, penetrative shortwave flux, and increased latent heat loss (Figures 8b–8e). TRMM satellite rainfall shows an increased precipitation rate associated with the cyclone (Figure 8f). The depth section of temperature from the moored observations shows a sudden appearance of subsurface warm waters at 30–60 m depths, which coincides with the arrival of the cyclone at the mooring location (Figure 9b). The penetrative shortwave radiation flux during 11–13 November was nearly zero suggesting that the subsurface warming was not due to local incident radiation and that it had to be an advective feature.

The salinity depth section shows a freshening event in the upper 25 m during 11–13 November (Figure 9c). The strong near-surface salinity stratification results in a shallow 10 m-deep mixed layer despite the strong cyclone winds. We compute the freshwater content in the upper 20 m using $FW_{20m} = \int_{-20}^{0} \left[1 - \frac{S(z)}{S_o}\right] dz$, where S(z)
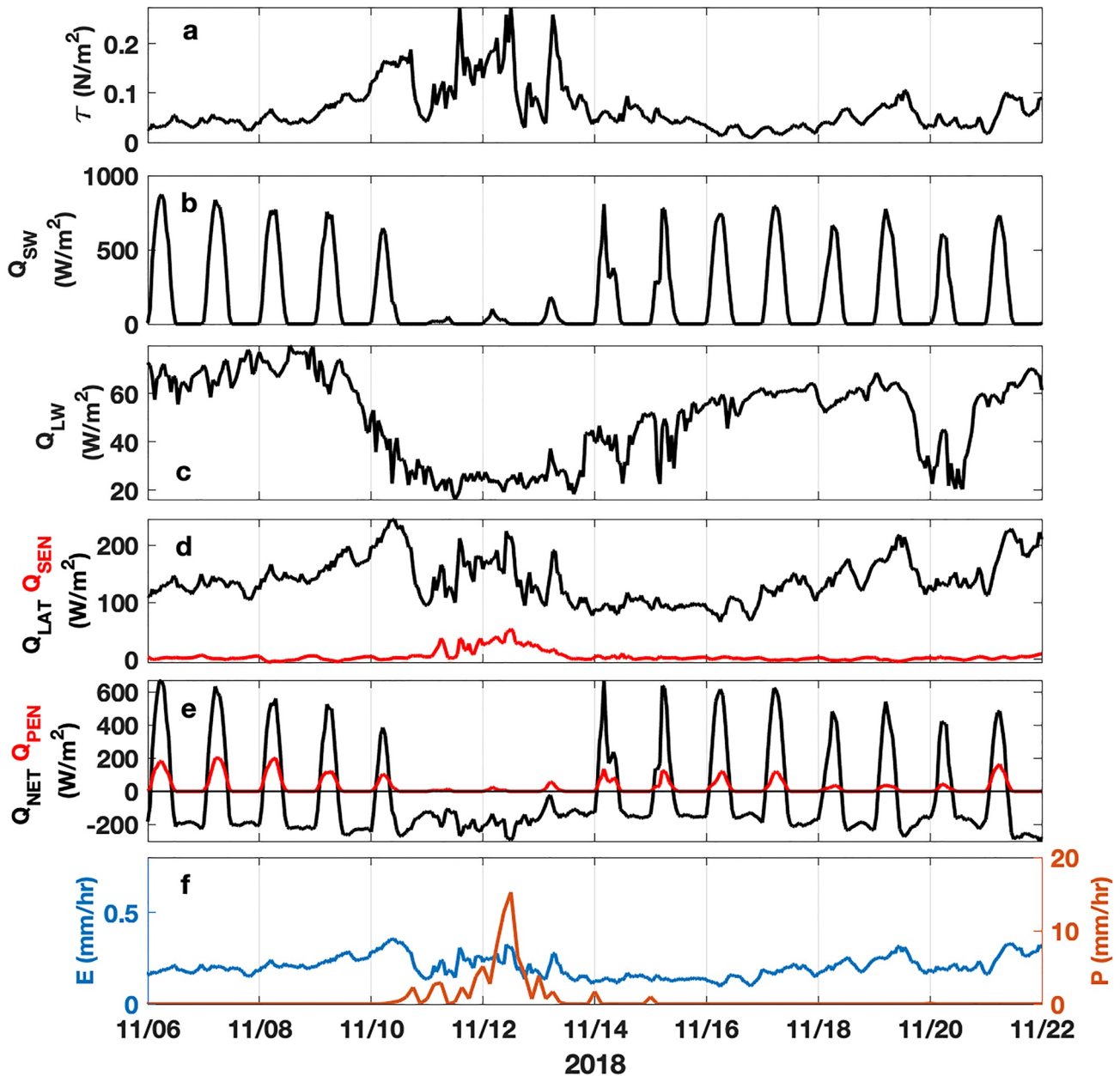
Figure 8. Hourly surface heat and freshwater fluxes observed at the 15°N, 90°E Research Moored Array for African-Asian-Australian Monsoon Analysis and Prediction mooring as in Figure 4 but during the passage of cyclone Gaja, 6–22 November 2018.

is the salinity at depth z and S_o is the reference salinity, taken as 35 pss. Freshwater content is defined as the amount of zero salinity water (in meters) that needs to be added to 35 pss ocean water to get the observed salinity. The freshening event results in a rise in the upper 20 m freshwater content of 0.9 m (Figure 9d). The time integral of precipitation (P) minus evaporation (E) or local freshwater forcing term $\int (P - E)dt$ cannot explain the rise in FW_{20m} suggesting that the drop in near-surface salinity occurs due to advection of freshwater to the mooring location. The mean vertical density ratio R at 10 m depth is 0.4 (<1), suggesting that the near-surface density stratification is mainly determined by salinity rather than temperature. This is the reason why the density structure looks similar to that of salinity in the upper 50 m (Figures 9c and 9e). The maps of SMAP SSS and AVISO geostrophic currents show that the Irrawaddy river water from the Andaman sea, and eastern BoB was advected by mesoscale eddy flow to the mooring location on 11 November 2018 (Figures 10a and 10b). The satellite SST maps show surface cooling by 1–2°C in the north and eastern Bay on 11 November as compared to the week before (Figures 10c and 10d). The shallow fresh layer and intense surface cooling led to the formation
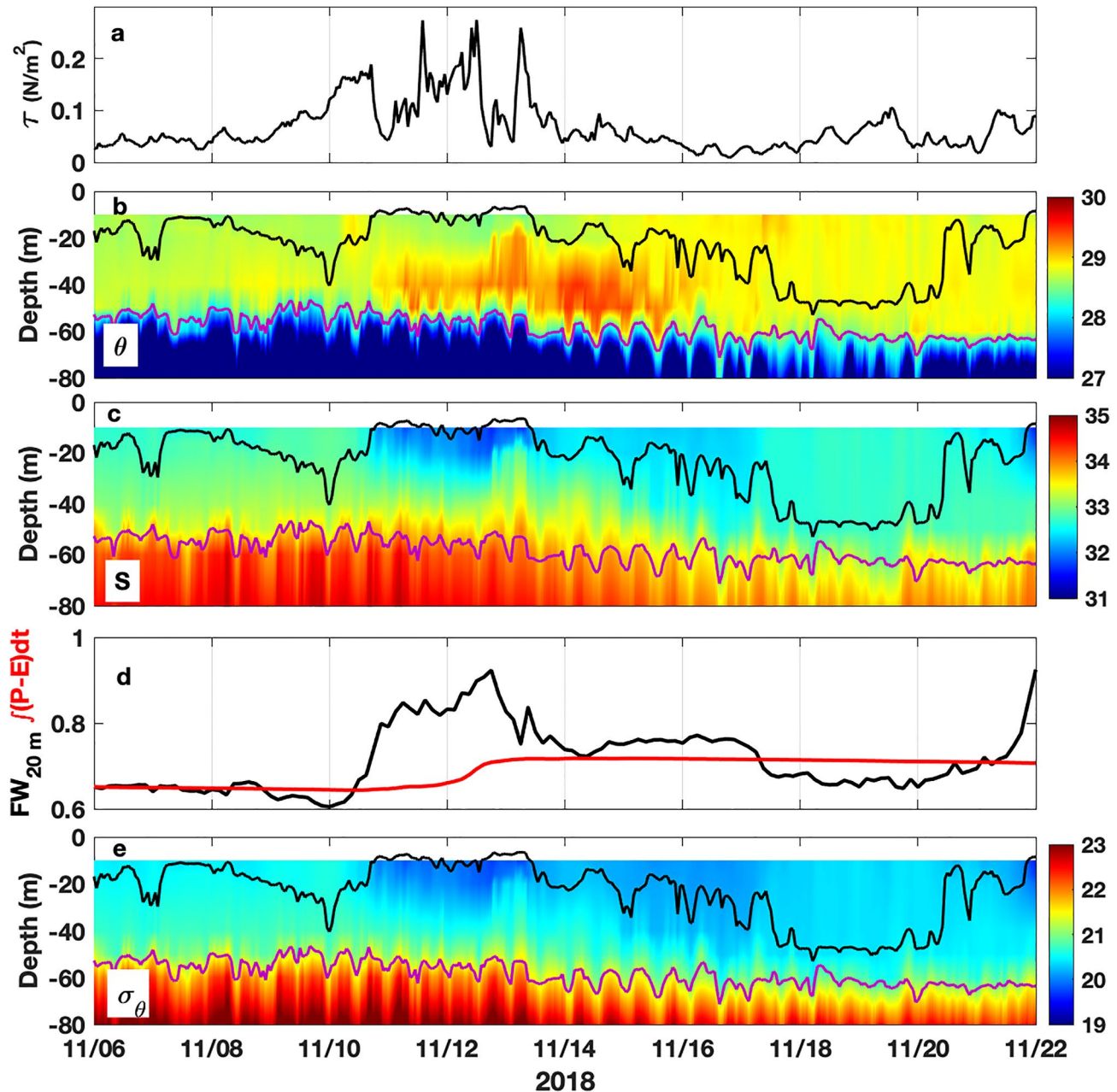
Figure 9. Moored observations of hourly (a) wind stress magnitude (τ; N m^{-2}), time-depth sections of (b) potential temperature (θ; °C), (c) salinity (S; pss), and (e) potential density (σ_θ; kg m^{-3}) during 6–22 November 2018. (d) Freshwater content (FW$_{20m}$; meters; black) and time integral of the local freshwater forcing term, precipitation minus evaporation (P–E; meters; red). The mixed layer depth (MLD; black) and isothermal layer depth (ILD; purple) and measurement depths (black dots) are shown in panels (b, c, and e). The semi-diurnal M2 tidal (12.5 hr) variability is prominent in temperature, salinity, and potential density at deeper depths below 40 m.

of subsurface thermal inversion. The global ocean analysis suggests that the river water in the eastern BoB was associated with a strong thermal inversion in the upper 40 m depth and a barrier layer more than 50 m thick that was advected to the mooring location (Figures 10e–10h). The thermal inversion persisted at the mooring for about 5 days from 11–16 November 2018. The barrier layer depth measured at the mooring is consistent with that of the global ocean analysis data.

The strong winds associated with cyclone Gaja generate strong near-inertial shear at the base of the mixed layer (Figure 11b). The stratification N^2 set up due to advection of shallow pool of river water with deep barrier layer dominates the velocity shear resulting in a high bulk Richardson Number Ri = 4.77 at 18 m depth during 11–13 November (Figure 11c). Strong near-inertial currents with an amplitude of about 0.1 m/s set up by the cyclone
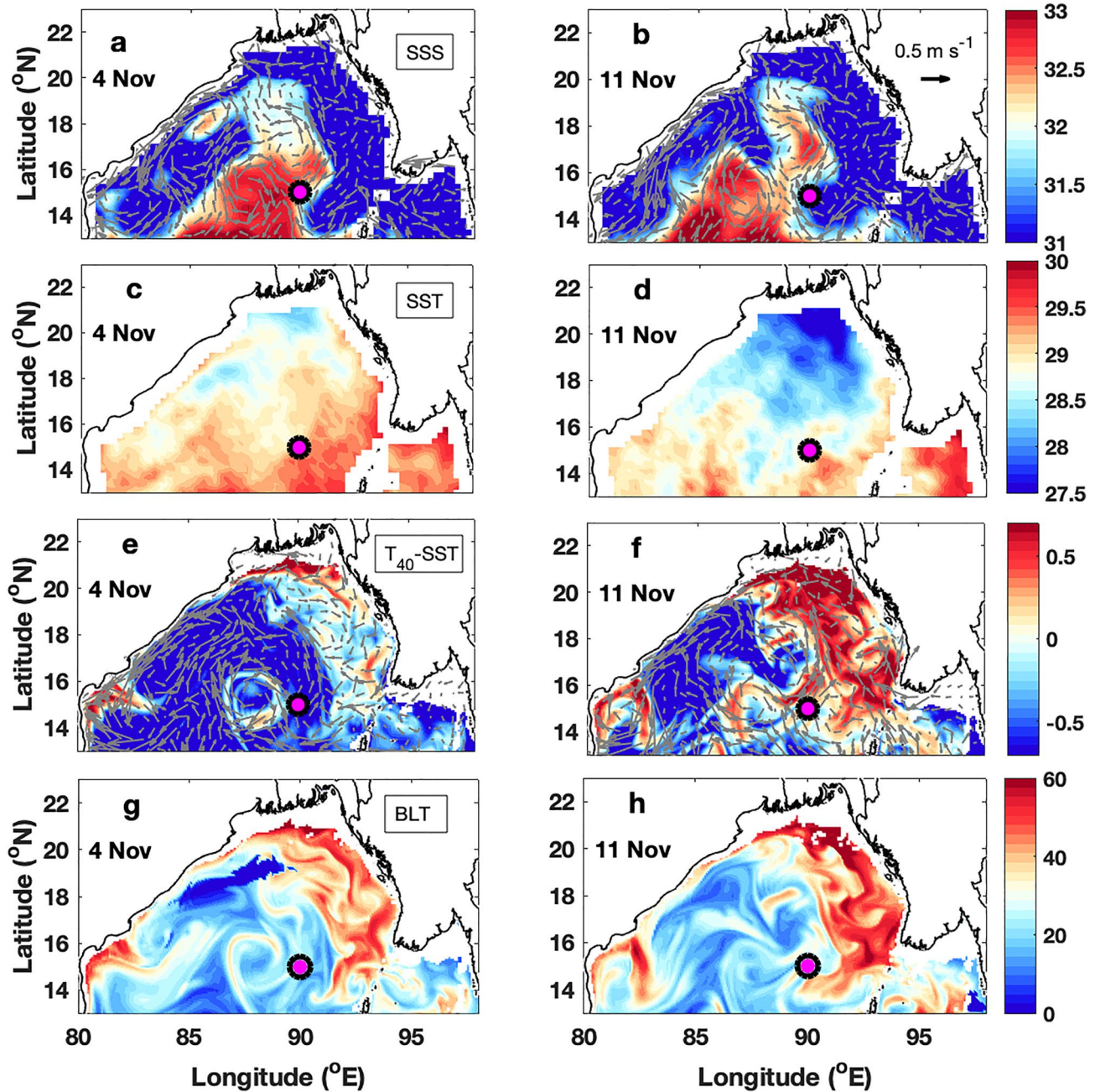
Figure 10. Spatial maps of daily 8-day running mean SMAP L3 v4 sea surface salinity (SSS; pss; color) and daily AVISO surface geostrophic currents (vectors) on (a) 4 November and (b) 11 November 2018. The 0.5 m s^{-1} reference vector is shown in panel (b). Spatial maps of daily satellite microwave sea surface temperature (SST; °C; color) on (c) 4 November and (d) 11 November 2018. Spatial maps of temperature difference (color) between 40 m depth and 0.46 m depth currents (vectors) from the Global Ocean Analysis data set on (e) 4 November and (f) 11 November 2018. (g and h) Barrier Layer Thickness (BLT; m; color) computed from Global Ocean Analysis data on 4 November and 11 November 2018, respectively. Location of 15°N, 90°E Research Moored Array for African-Asian-Australian Monsoon Analysis and Prediction mooring (pink dot) is shown.

winds act to eventually deepen the mixed layer on 14 November after the cyclone has passed. The mean wind stress magnitude during 14–20 November was nearly zero but the mixed layer deepened to about 40 m depth during this period. The mixed layer deepening resulted in increase of about 0.5 pss in surface salinity and 0.8°C rise in SST at the mooring location. The bulk mean Ri was 0.46 at 30 m depth suggesting strong shear-driven mixing and the reduced shear was positive (Figure 11d). The depth section of inertial zonal current shows upward phase propagation suggesting downward energy propagation during 14–20 November (Figure 11e). It is also very
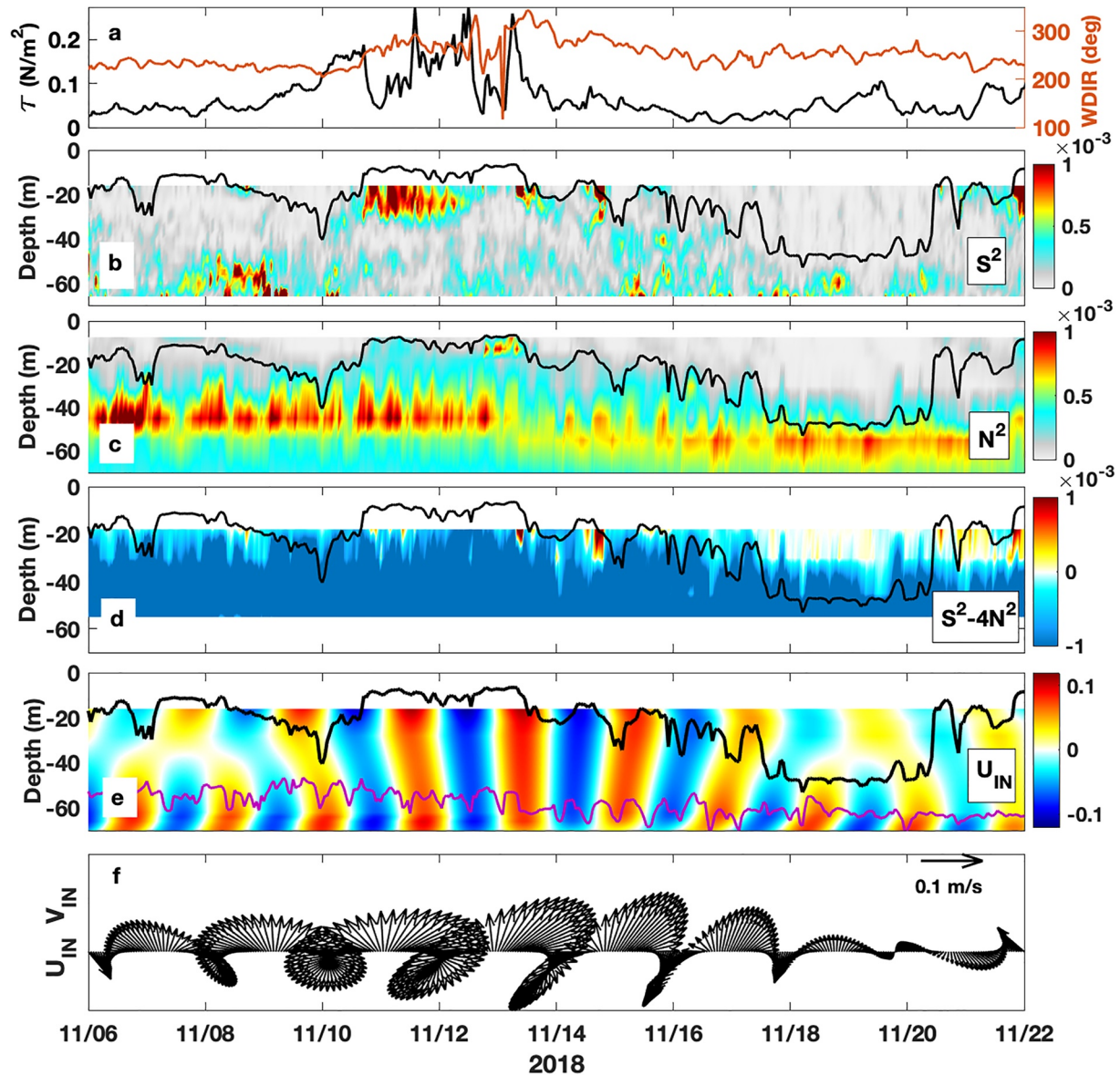
Figure 11. Moored observations of hourly (a) wind stress magnitude (τ; N m^{-2}; black) and wind direction (degrees; orange), time-depth sections of (b) shear-squared (S^2; s^{-2}), (c) Brunt-vaisala frequency squared (N^2; s^{-2}), (d) reduced shear ($S^2 - 4 N^2$; s^{-2}), and (e) inertial zonal velocity (U_{IN}; m s^{-1}). MLD (m; black line) and ILD (m; purple line) are shown in panels (b–e). (f) Vector plot of zonal (U_{IN}; m s^{-1}) and meridional (V_{IN}; m s^{-1}) inertial currents during 6–22 November 2018 at 15°N, 90°E. A reference current vector of 0.1 m s^{-1} is shown.

interesting to note that the near-inertial currents generated by cyclone Gaja are much higher in amplitude than in the case of cyclone Titli though the winds associated with Titli were more intense. The reason could be the sudden shift in the wind speed and direction during passage of cyclone Gaja over one inertial period resulting from the looping of the cyclone track (Figure 11a). Pollard and Millard (1970) suggest that a wind vector blowing in one direction during an inertial period would not generate inertial current as the momentum added during the first half period would be removed by it during the second half period. On the other hand, strong winds with a sudden shift in the direction within an inertial period would be more efficient in generating inertial oscillations (Figure 11a and 11f).

3.2.1. Mixed Layer Heat and Salt Balance

Figure 12 shows the mixed layer salt and heat balance terms estimated using the moored observations together with SMAP satellite SSS and microwave OISST data as discussed in Section 3.1.1. We observe freshening of
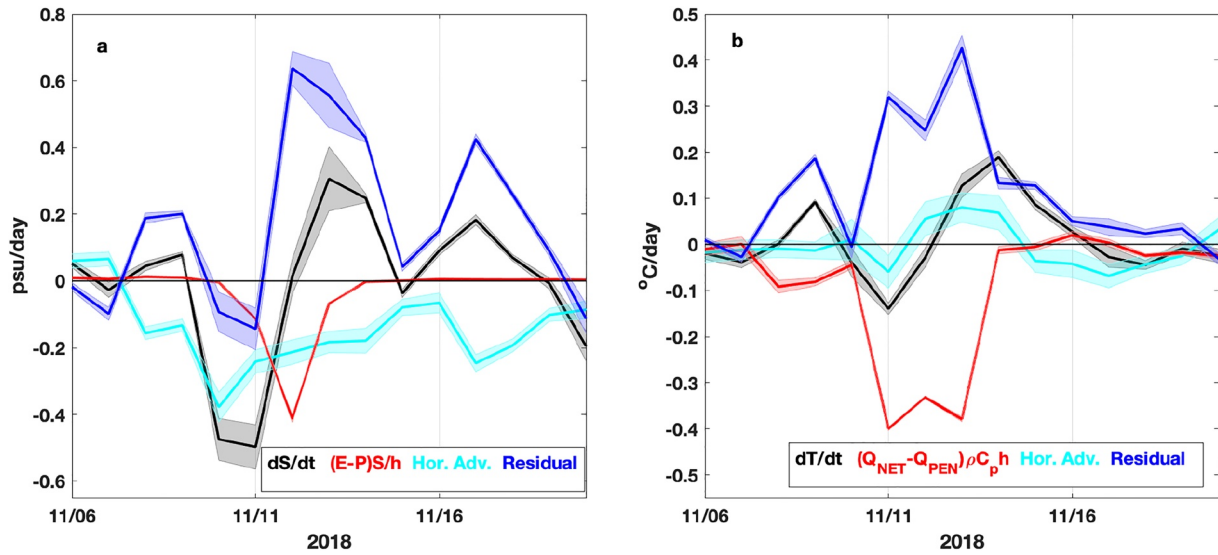
Figure 12. (a) Daily estimates of the rate of change in mixed layer salinity (dS/dt; black), freshwater forcing ($\frac{(E-P)S}{h}$; red), horizontal advection (cyan) and residual (blue) terms in the mixed layer salt balance equation during 6–19 November 2018. Units in pss day^{-1}. (b) Daily estimates of rate of change in mixed layer temperature (dT/dt; black), surface heat forcing ($\frac{Q_{net}-Q_{pen}}{\rho C_p h}$; red), horizontal advection (cyan), and residual (blue) terms in the mixed layer heat balance equation. Units in °C day^{-1}. Shading in (a) and (b) represents one standard error in each term. We estimate the standard error of each term in the balance equations on a single day conservatively as the standard deviation of the 24 hourly values for that particular day.

the mixed layer at the mooring by 0.5 pss/day during the passage of cyclone Gaja. This freshening during 10–12 November is explained by the horizontal advection term with very little contribution from the local freshwater forcing. The rise in SSS during 14–20 November after the passage of the cyclone was mainly due to the residual term suggesting that mixing of saltier water from deeper depths into the mixed layer occurred as the mixed layer deepened to about 40 m depth. The heat balance suggests that near-surface cooling of 0.4°C/day during the passage of cyclone Gaja resulted from horizontal advection as well as net heat loss from the surface. SST warming at the rate of 0.2°C day^{-1} after the passage of cyclone is explained by the residual term. The mixed layer temperature tendency indicates increasing SST during 13–16 November consistent with the residual, which suggests mixing of subsurface warm water into the mixed layer by shear associated with inertial currents set up by the cyclone winds.

4. Summary

This study uses a combination of the moored observations, satellite retrievals, and ocean analysis data sets to study the upper ocean response and mixed layer salinity and temperature evolution at 15°N, 90°E under the influence of forcing from two very severe post-monsoon cyclones, Titli and Gaja, that occurred in the Bay of Bengal during October–November 2018. Prior to the development of cyclone Titli, the entire north Bay was subjected to 2–3°C warming due to clear skies and calm wind conditions following a break period in the summer monsoon toward the end of September. This resulted in a very shallow mixed layer and a build-up of strong near-surface thermal stratification at the mooring location. During the passage of cyclone Titli, the temperature-dominated density stratification restricted the mixed layer deepening to the upper 25 m depth despite the strong cyclone winds. The shallow mixing led to cooling of SST by 2°C with a weak rise (less than 0.1 pss day^{-1}) in the mixed layer salinity. The ADCP velocity measurements showed cyclone-forced inertial currents with an amplitude of 0.8 m s^{-1} in the mixed layer and below that decayed in about 2 days after the cyclone passage. The mixed layer heat balance suggests that SST cooling during 7–11 October was mainly due to net heat loss from the surface and the mixing due to shear associated with the inertial currents.

During the passage of cyclone Gaja, a shallow 20 m pool of river water was advected to the 15°N mooring by mesoscale eddy flow. This pool of river water was also associated with a subsurface warm layer and a thick barrier layer. The strong near-surface density stratification associated with the freshwater restricted vertical mixing under the strong cyclone winds. Chaudhuri et al. (2019) used a one-dimensional PWP model for a case

study of post-monsoon cyclone Phailin (8–13 October 2013) in the BoB to show that the preexisting salinity stratification reduces the maximum depth of storm-induced mixing by at least 50%. Looping of the track of cyclone Gaja during 11–13 November resulted in rapid changes in the wind speed and direction, which led to the generation of strong near-inertial currents in the mixed layer that penetrated into thermocline. We observe an upward phase propagation in the zonal inertial currents suggesting downward energy propagation from the mixed layer to thermocline. The amplitude of the near-inertial currents weakened in about 8 days after the cyclone passage. The decay time scale of near-inertial currents in the case of cyclone Gaja was longer than for cyclone Titli where the inertial currents decayed in about 2 days (Figures 6 and 11). The shear associated with inertial currents acts to deepen the mixed layer to about 40 m depth during 14–18 November, after the cyclone passed. The mixed layer salt balance shows that horizontal advection was dominant in freshening the mixed layer at the mooring location during the cyclone passage. Increase in mixed layer salinity after the cyclone passage can be explained mainly by the residual mixing term. The mixed layer heat balance also shows dominance of the residual mixing term in increasing the SST after the passage of cyclone. Unlike the case of cyclone Titli, due to the presence of thermal inversion and deep barrier layer, we do not observe a distinct cold wake along the track of cyclone Gaja consistent with Chaudhuri et al. (2019) who showed that the presence of a deep warm barrier layer can reduce the SST cooling under tropical cyclones by a factor of 2.5. Previous studies showed that the absence of SST cooling under post-monsoon cyclones in the BoB leads to further intensification of cyclones (Balaguru et al., 2012; Neetu et al., 2012; Sengupta et al., 2008). The oceanic response was different for both Titli and Gaja primarily because of the differences in the ocean pre-conditioning. In case of Titli, near-surface thermal stratification restricted mixed layer deepening to 25 m depth and limited SST cooling. In case of cyclone Gaja, strong salinity-dominated stratification and presence of a subsurface warm layer associated with the Irrawaddy River water restricted vertical mixing under the cyclone. The mixed layer deepened to 40 m depth after the cyclone passage resulting in warm SST. A previous study by Navaneeth et al. (2019) used moored buoy and satellite observations to compare the ocean response to October cyclones Phailin and Hudhud, which occurred in the Bay of Bengal in 2013 and 2014, respectively. They found that a thermal inversion supported by preexisting strong near-surface salinity stratification restricted vertical mixing and SST cooling along the track of Phailin, while a weaker thermal stratification prior to cyclone Hudhud resulted in SST cooling of about 1.5°C in magnitude.

This observational study in the north Bay of Bengal demonstrates the importance of ocean preconditioning and upper ocean thermohaline stratification in the evolution of mixed layer temperature and salinity under the influence of post-monsoon cyclones in the Bay of Bengal. We note however some limitations of our study: (a) there was only one fully instrumented RAMA mooring in 2018–2019 from which we could perform detailed surface layer diagnostics in the Bay of Bengal; (b) temperature, salinity, and velocity fields in the upper 20–40 m were coarsely resolved in the vertical with no velocity data in the upper 16 m; and (c) errors in the residual terms estimated from the mixed layer heat and salt balances were relatively large because the horizontal advection terms were estimated using a combination of mooring and coarsely resolved satellite observations. This is more of problem with the salinity balance because of the 70 km resolution of SMAP. Addressing these shortcomings in future studies is essential. With increasing frequency and intensity of post-monsoon cyclones in the warming climate (Balaguru et al., 2014), it is very important to understand the ocean mixed layer response and associated air-sea interactions during these cyclones. A better understanding of the key processes can help improve the prediction of cyclone tracks and intensity in the future, which will have tremendous value to people living in the region under threat from cyclone hazards.

Data Availability Statement

The 15°N RAMA mooring data are publicly available at https://www.pmel.noaa.gov/tao/drupal/disdel; The daily TRMM 3B42v7 satellite rainfall data are at https://disc.gsfc.nasa.gov/datasets/TRMM_3B42_Daily_7/summary; AVISO sea surface geostrophic currents www.aviso.altimetry.fr/en/data/; Argo float data at https://www.nodc.noaa.gov/argo/; SMAP satellite sea surface salinity data at https://www.remss.com/missions/smap/; Satellite microwave OISST is at https://www.remss.com/measurements/sea-surface-temperature/; Global ocean analysis (Global_Analysis_Forecast_PHY_001_030) at http://marine.copernicus.eu/.

References

Alam, M. M., Hossain, M. A., & Shafee, S. (2003). Frequency of Bay of Bengal cyclonic storms and depressions crossing different coastal zones. *International Journal of Climatology: A Journal of the Royal Meteorological Society*, *23*(9), 1119–1125. https://doi.org/10.1002/joc.927

Balaguru, K., Chang, P., Saravanan, R., Leung, L. R., Xu, Z., Li, M., & Hsieh, J. S. (2012). Ocean barrier layers' effect on tropical cyclone intensification. *Proceedings of the National Academy of Sciences*, *109*(36), 14343–14347. https://doi.org/10.1073/pnas.1201364109

Balaguru, K., Taraphdar, S., Leung, L. R., & Foltz, G. R. (2014). Increase in the intensity of postmonsoon Bay of Bengal tropical cyclones. *Geophysical Research Letters*, *41*(10), 3594–3601. https://doi.org/10.1002/2014gl060197

Chassignet, E. P., Pascual, A., Tintore, J., & Verron, J. (Eds.) (2018). *New frontiers in operational oceanography*. GODAE Oceanview.

Chaudhuri, D., Sengupta, D., D'Asaro, E., Venkatesan, R., & Ravichandran, M. (2019). Response of the salinity-stratified Bay of Bengal to cyclone Phailin. *Journal of Physical Oceanography*, *49*(5), 1121–1140. https://doi.org/10.1175/jpo-d-18-0051.1

Cole, S. T., Rudnick, D. L., & Colosi, J. A. (2010). Seasonal evolution of upper-ocean horizontal structure and the remnant mixed layer. *Journal of Geophysical Research*, *115*(C4), C04012. https://doi.org/10.1029/2009jc005654

D'Asaro, E. A. (1985). The energy flux from the wind to near-inertial motions in the surface mixed layer. *Journal of Physical Oceanography*, *15*(8), 1043–1059. https://doi.org/10.1175/1520-0485(1985)015<1043:tefftw>2.0.co;2

D'Asaro, E. A. (2003). The ocean boundary layer below Hurricane Dennis. *Journal of Physical Oceanography*, *33*(3), 561–579. https://doi.org/10.1175/1520-0485(2003)033<0561:toblbh>2.0.co;2

Emanuel, K. A. (1999). Thermodynamic control of hurricane intensity. *Nature*, *401*(6754), 665–669. https://doi.org/10.1038/44326

Figueroa, H. A. (1996). World ocean density ratios. *Journal of Physical Oceanography*, *26*(2), 267–275. https://doi.org/10.1175/1520-0485(1996)026<0267:wodr>2.0.co;2

Foltz, G. R., & McPhaden, M. J. (2008). Seasonal mixed layer salinity balance of the tropical North Atlantic Ocean. *Journal of Geophysical Research*, *113*(C2), C02013. https://doi.org/10.1029/2007jc004178

Fore, A. G., Yueh, S. H., Tang, W., Stiles, B. W., & Hayashi, A. K. (2016). Combined active/passive retrievals of ocean vector wind and sea surface salinity with SMAP. *IEEE Transactions on Geoscience and Remote Sensing*, *54*(12), 7396–7404. https://doi.org/10.1109/tgrs.2016.2601486

Freitag, H. P., Ning, C., Berk, P., Dougherty, D., Marshall, R., Strick, J. M., & Zimmerman, D. (2016). *ATLAS, T-Flex, BaiLong meteorological sensor comparison test report (NOAA Technical Memorandum OAR PMEL-148)*. NOAA Pacific Marine Environmental Laboratory.

Freitag, H. P., O'Haleck, M., Thomas, G. C., & McPhaden, M. J. (2001). *Calibration procedures and instrumental accuracies for ATLAS wind measurements (NOAA Technical Memorandum OAR PMEL-119)*. NOAA Pacific Marine Environmental Laboratory.

Girishkumar, M. S., Joseph, J., Thangaprakash, V. P., Pottapinjara, V., & McPhaden, M. J. (2017). Mixed layer temperature budget for the northward propagating summer monsoon intraseasonal oscillation (MISO) in the central Bay of Bengal. *Journal of Geophysical Research: Oceans*, *122*(11), 8841–8854. https://doi.org/10.1002/2017jc013073

Girishkumar, M. S., & Ravichandran, M. (2012). The influences of ENSO on tropical cyclone activity in the Bay of Bengal during October–December. *Journal of Geophysical Research*, *117*(C2). https://doi.org/10.1029/2011jc007417

Girishkumar, M. S., Suprit, K., Vishnu, S., Prakash, V. P., & Ravichandran, M. (2015). The role of ENSO and MJO on rapid intensification of tropical cyclones in the Bay of Bengal during October–December. *Theoretical and Applied Climatology*, *120*(3), 797–810. https://doi.org/10.1007/s00704-014-1214-z

Huffman, G. J., Bolvin, D. T., Nelkin, E. J., Wolff, D. B., Adler, R. F., Gu, G., et al. (2007). The TRMM multisatellite precipitation analysis (TMPA): Quasi-global, multiyear, combined-sensor precipitation estimates at fine scales. *Journal of Hydrometeorology*, *8*(1), 38–55. https://doi.org/10.1175/jhm560.1

IMD Report. (2018). *Report on cyclonic disturbances over north Indian Ocean during 2018* (pp. 178–204). Indian Meteorological Department, Technical Report.

Jyoteeshkumar Reddy, P., Sriram, D., Gunthe, S. S., & Balaji, C. (2021). Impact of climate change on intense Bay of Bengal tropical cyclones of the post-monsoon season: A pseudo global warming approach. *Climate Dynamics*, *56*(9), 2855–2879. https://doi.org/10.1007/s00382-020-05618-3

Kumar, B. P., D'Asaro, E., & Ravichandran, M. (2019). Widespread cooling of the Bay of Bengal by tropical storm Roanu. *Deep Sea Research Part II: Topical Studies in Oceanography*, *168*, 104652. https://doi.org/10.1016/j.dsr2.2019.104652

Kurian, J., & Vinayachandran, P. N. (2006). Formation mechanisms of temperature inversions in the southeastern Arabian Sea. *Geophysical Research Letters*, *33*(17), L17611. https://doi.org/10.1029/2006gl027280

Li, Z., Yu, W., Li, T., Murty, V. S. N., & Tangang, F. (2013). Bimodal character of cyclone climatology in the Bay of Bengal modulated by monsoon seasonal cycle. *Journal of Climate*, *26*(3), 1033–1046. https://doi.org/10.1175/jcli-d-11-00627.1

Lin, I., Liu, W. T., Wu, C. C., Wong, G. T., Hu, C., Chen, Z., et al. (2003). New evidence for enhanced ocean primary production triggered by tropical cyclone. *Geophysical Research Letters*, *30*(13). https://doi.org/10.1029/2003gl017141

Lin, I. I., Chen, C. H., Pun, I. F., Liu, W. T., & Wu, C. C. (2009). Warm ocean anomaly, air sea fluxes, and the rapid intensification of tropical cyclone Nargis (2008). *Geophysical Research Letters*, *36*(3). https://doi.org/10.1029/2008gl035815

Maneesha, K., Murty, V. S. N., Ravichandran, M., Lee, T., Yu, W., & McPhaden, M. J. (2012). Upper ocean variability in the Bay of Bengal during the tropical cyclones Nargis and Laila. *Progress in Oceanography*, *106*, 49–61. https://doi.org/10.1016/j.pocean.2012.06.006

Maneesha, K., Prasad, V. S., & Venkateswararao, K. (2021). Ocean impact on the intensification of cyclone Titli. *Journal of Earth System Science*, *130*(3), 1–9. https://doi.org/10.1007/s12040-021-01660-9

McPhaden, M. J., Foltz, G. R., Lee, T., Murty, V. S. N., Ravichandran, M., Vecchi, G. A., et al. (2009). Ocean-atmosphere interactions during cyclone Nargis. *EOS, Transactions American Geophysical Union*, *90*(7), 53–54. https://doi.org/10.1029/2009eo070001

McPhaden, M. J., Meyers, G., Ando, K., Masumoto, Y., Murty, V. S. N., Ravichandran, M., et al. (2009). RAMA: The research moored Array for African-Asian-Australian monsoon analysis and prediction. *Bulletin of the American Meteorological Society*, *90*(4), 459–480. https://doi.org/10.1175/2008bams2608.1

Mickett, J. B., Serra, Y. L., Cronin, M. F., & Alford, M. H. (2010). Resonant forcing of mixed layer inertial motions by atmospheric easterly waves in the northeast tropical Pacific. *Journal of Physical Oceanography*, *40*(2), 401–416. https://doi.org/10.1175/2009jpo4276.1

Mohanty, U. C., Nadimpalli, R., & Mohanty, S. (2021). Understanding the rapid intensification of tropical cyclone Titli using Hurricane WRF model simulations. *MAUSAM*, *72*(1), 167–176. https://doi.org/10.54302/mausam.v72i1.129

Mohanty, U. C., Osuri, K. K., Pattanayak, S., & Sinha, P. (2012). An observational perspective on tropical cyclone activity over Indian seas in a warming environment. *Natural Hazards*, *63*(3), 1319–1335. https://doi.org/10.1007/s11069-011-9810-z

Navaneeth, K. N., Martin, M. V., Joseph, K. J., & Venkatesan, R. (2019). Contrasting the upper ocean response to two intense cyclones in the Bay of Bengal. *Deep Sea Research Part I: Oceanographic Research Papers*, *147*, 65–78. https://doi.org/10.1016/j.dsr.2019.03.010

Neetu, S., Lengaigne, M., Vincent, E. M., Vialard, J., Madec, G., Samson, G., et al. (2012). Influence of upper-ocean stratification on tropical cyclone-induced surface cooling in the Bay of Bengal. *Journal of Geophysical Research*, *117*(C12). https://doi.org/10.1029/2012jc008433

Parampil, S., Bharathraj, G. N., Harrison, M., & Sengupta, D. (2016). Observed subseasonal variability of heat flux and the SST response of the tropical Indian Ocean. *Journal of Geophysical Research: Oceans*, *121*(10), 7290–7307. https://doi.org/10.1002/2016jc011948

Pasquero, C., Desbiolles, F., & Meroni, A. N. (2021). Air-sea interactions in the cold wakes of tropical cyclones. *Geophysical Research Letters*, *48*(2), e2020GL091185. https://doi.org/10.1029/2020gl091185

Paulson, C. A., & Simpson, J. J. (1977). Irradiance measurements in the upper ocean. *Journal of Physical Oceanography*, *7*(6), 952–956. https://doi.org/10.1175/1520-0485(1977)007<0952:imituo>2.0.co;2

Plimpton, P. E., Freitag, H. P., & McPhaden, M. J. (1997). ADCP velocity errors from pelagic fish schooling around equatorial moorings. *Journal of Atmospheric and Oceanic Technology*, *14*(5), 1212–1223. https://doi.org/10.1175/1520-0426(1997)014<1212:avefpf>2.0.co;2

Plimpton, P. E., Freitag, H. P., & McPhaden, M. J. (2004). Processing of subsurface ADCP data in the equatorial Pacific.

Pollard, R. T., & Millard, R. C., Jr. (1970). Comparison between observed and simulated wind-generated inertial oscillations. In *Deep sea research and Oceanographic Abstracts* (Vol. 17, pp. 813–821). Elsevier. https://doi.org/10.1016/0011-7471(70)90043-4

Price, J. F. (1981). Upper ocean response to a hurricane. *Journal of Physical Oceanography*, *11*(2), 153–175. https://doi.org/10.1175/1520-0485(1981)011<0153:uortah>2.0.co;2

Rao, R. R., & Sivakumar, R. (2003). Seasonal variability of sea surface salinity and salt budget of the mixed layer of the North Indian Ocean. *Journal of Geophysical Research*, *108*(C1), 9–1. https://doi.org/10.1029/2001jc000907

Rudnick, D. L., & Ferrari, R. (1999). Compensation of horizontal temperature and salinity gradients in the ocean mixed layer. *Science*, *283*(5401), 526–529. https://doi.org/10.1126/science.283.5401.526

Saraceno, M., Strub, P. T., & Kosro, P. M. (2008). Estimates of sea surface height and near-surface alongshore coastal currents from combinations of altimeters and tide gauges. *Journal of Geophysical Research*, *113*(C11), C11013. https://doi.org/10.1029/2008jc004756

Scannell, H. A., & McPhaden, M. J. (2018). Seasonal mixed layer temperature balance in the southeastern tropical Atlantic. *Journal of Geophysical Research: Oceans*, *123*(8), 5557–5570. https://doi.org/10.1029/2018jc014099

Sengupta, D., Bharath Raj, G. N., Ravichandran, M., Sree Lekha, J., & Papa, F. (2016). Near-surface salinity and stratification in the North Bay of Bengal from moored observations. *Geophysical Research Letters*, *43*(9), 4448–4456. https://doi.org/10.1002/2016gl068339

Sengupta, D., Bharath Raj, G. N., & Shenoi, S. S. C. (2006). Surface freshwater from Bay of Bengal runoff and Indonesian throughflow in the tropical Indian Ocean. *Geophysical Research Letters*, *33*(22), L22609. https://doi.org/10.1029/2006gl027573

Sengupta, D., Goddalehundi, B. R., & Anitha, D. S. (2008). Cyclone-induced mixing does not cool SST in the post-monsoon North Bay of Bengal. *Atmospheric Science Letters*, *9*(1), 1–6. https://doi.org/10.1002/asl.162

Shroyer, E. L., Gordon, A. L., Jaeger, G. S., Freilich, M., Waterhouse, A. F., Farrar, J. T., et al. (2020). Upper layer thermohaline structure of the Bay of Bengal during the 2013 northeast monsoon. *Deep Sea Research Part II: Topical Studies in Oceanography*, *172*, 104630. https://doi.org/10.1016/j.dsr2.2019.07.018

Singh, O. P., Khan, A., & Rahman, M. S. (2000). Changes in the frequency of tropical cyclones over the North Indian Ocean. *Meteorology and Atmospheric Physics*, *75*(1), 11–20. https://doi.org/10.1007/s007030070011

Sree Lekha, J., Buckley, J. M., Tandon, A., & Sengupta, D. (2018). Subseasonal dispersal of freshwater in the northern Bay of Bengal in the 2013 summer monsoon season. *Journal of Geophysical Research: Oceans*, *123*(9), 6330–6348. https://doi.org/10.1029/2018jc014181

Sree Lekha, J., Lucas, A. J., Sukhatme, J., Joseph, J. K., Ravichandran, M., Suresh Kumar, N., et al. (2020). Quasi-biweekly mode of the Asian summer monsoon Revealed in Bay of Bengal surface observations. *Journal of Geophysical Research: Oceans*, *125*(12), e2020JC016271. https://doi.org/10.1029/2020jc016271

Thadathil, P., Gopalakrishna, V. V., Muraleedharan, P. M., Reddy, G. V., Araligidad, N., & Shenoy, S. (2002). Surface layer temperature inversion in the Bay of Bengal. *Deep Sea Research Part I: Oceanographic Research Papers*, *49*(10), 1801–1818. https://doi.org/10.1016/s0967-0637(02)00044-4

Thadathil, P., Suresh, I., Gautham, S., Prasanna Kumar, S., Lengaigne, M., Rao, R. R., et al. (2016). Surface layer temperature inversion in the Bay of Bengal: Main characteristics and related mechanisms. *Journal of Geophysical Research: Oceans*, *121*(8), 5682–5696. https://doi.org/10.1002/2016jc011674

Thangaprakash, V. P., Girishkumar, M. S., Suprit, K., Kumar, N. S., Chaudhuri, D., Dinesh, K., et al. (2016). What controls seasonal evolution of sea surface temperature in the Bay of Bengal? Mixed layer heat budget analysis using moored buoy observations along 90 E. *Oceanography*, *29*(2), 202–213. https://doi.org/10.5670/oceanog.2016.52

Tiwari, G., Rameshan, A., Kumar, P., Javed, A., & Mishra, A. K. (2022). Understanding the post-monsoon tropical cyclone variability and trend over the Bay of Bengal during the satellite era. *Quarterly Journal of the Royal Meteorological Society*, *148*(742), 1–14. https://doi.org/10.1002/qj.4189

Udaya Bhaskar, T. V., Jayaram, C., & Rama Rao, E. P. (2013). Comparison between Argo-derived sea surface temperature and microwave sea surface temperature in tropical Indian Ocean. *Remote sensing letters*, *4*(2), 141–150. https://doi.org/10.1080/2150704x.2012.711955

Venkatesan, R., Mathew, S., Vimala, J., Latha, G., Muthiah, M. A., Ramasundaram, S., & Atmanand, M. A. (2014). Signatures of very severe cyclonic storm Phailin in met–ocean parameters observed by moored buoy network in the Bay of Bengal. *Current Science*, 589–595.

Vijay Prakash, K., Vimala, G., Ch, S., Nagamani, P. V., Baranval, N. K., Manche, S., et al. (2021). Role of physical oceanography parameters in ocean's biological response during the passage of cyclone Titli in the Bay of Bengal. *Journal of Earth System Science*, *130*(3), 1–12. https://doi.org/10.1007/s12040-021-01625-y

Vissa, N. K., Satyanarayana, A. N. V., & Prasad Kumar, B. (2013). Intensity of tropical cyclones during pre-and post-monsoon seasons in relation to accumulated tropical cyclone heat potential over Bay of Bengal. *Natural Hazards*, *68*(2), 351–371. https://doi.org/10.1007/s11069-013-0625-y

Yu, L., & McPhaden, M. J. (2011). Ocean preconditioning of Cyclone Nargis in the Bay of Bengal: Interaction between Rossby waves, surface fresh waters, and sea surface temperatures. *Journal of Physical Oceanography*, *41*(9), 1741–1755. https://doi.org/10.1175/2011jpo4437.1

Zedler, S. E., Dickey, T. D., Doney, S. C., Price, J. F., Yu, X., & Mellor, G. L. (2002). Analyses and simulations of the upper ocean's response to hurricane Felix at the Bermuda testbed mooring site: 13–23 August 1995. *Journal of Geophysical Research*, *107*(C12), 25–31. https://doi.org/10.1029/2001jc000969